LANGMUIR

pubs.acs.org/Langmuir

Invited Feature Article

Liquid Optothermoelectrics: Fundamentals and Applications

Zhihan Chen, Pavana Siddhartha Kollipara, Hongru Ding, Agatian Pughazhendi, and Yuebing Zheng*

Cite This: *Langmuir* 2021, 37, 1315−1336

Read Online

ACCESS | Metrics & More | Article Recommendations

ABSTRACT: Liquid thermoelectricity describes the redistribution of ions in an electrolytic solution under the influence of temperature gradients, which leads to the formation of electric fields. The thermoelectric field is effective in driving the thermophoretic migration of charged colloidal particles for versatile manipulation. However, traditional macroscopic thermoelectric fields are not suitable for particle manipulations at high spatial resolution. Inspired by optical tweezers and relevant optical manipulation techniques, we employ laser interaction with light-absorbing nanostructures to achieve subtle heat management on the micro- and nanoscales. The resulting thermoelectric fields are exploited to develop new optical technologies, leading to a research field known as liquid optothermoelectrics. This Invited Feature Article highlights our recent works on advancing fundamentals, technologies, and applications of optothermoelectrics in colloidal solutions. The effects of light irradiation, substrates, electrolytes, and particles on the optothermoelectric manipulations of colloidal particles along with their theoretical limitations are discussed in detail. Our optothermoelectric technologies with the versatile capabilities of trapping, manipulating, and pulling colloidal particles at low optical power are finding applications in microswimmers and nanoscience. With its intricate interfacial processes and tremendous technological promise, optothermoelectrics in colloidal solutions will remain relevant for the foreseeable future.

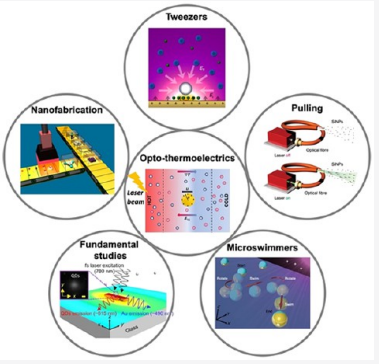

Downloaded via UNIV OF TEXAS AT AUSTIN on June 19, 2021 at 15:12:36 (UTC).
See https://pubs.acs.org/sharingguidelines for options on how to legitimately share published articles.

INTRODUCTION

When a colloidal system is subject to a temperature gradient, the suspended colloidal particles migrate directionally because of thermophoresis. In the past two decades, several studies have revealed that colloidal particles can drift toward the cold region or hot region depending on the electrolyte composition.[1−3] The electrolyte-dependent thermophobicity and thermophilicity of colloidal particles are attributed to thermoelectricity, namely, the Seebeck effect or thermoelectric effect, in the electrolyte solution.[4−7] Briefly, ions with different Soret coefficients under a temperature gradient drift differently and experience spatial separation in the electrolyte solution, which leads to a steady thermoelectric field that can influence the thermophoretic motion of the suspended charged particles. As thermoelectricity is widely applicable to diverse charged particles and can be tuned as a function of the electrolyte composition,[2] ionic strength,[8] temperature,[9,10] particle−solvent interface,[11] colloidal size,[12] and particle concentration,[13,14] the principles of thermoelectricity have been exploited here to achieve versatile manipulations of colloidal particles.

To manipulate colloidal particles based on the thermoelectric effect with high spatial resolution, the localized temperature gradient field in the vicinity of the particles needs to be controllable. Inspired by the precise manipulation of colloidal particles via optical tweezers and other relevant optical techniques,[15−18] we couple the optothermal effect and the resultant thermoelectric field to achieve optothermoelectric manipulations at the micro- and nanoscales. Through engineering the shape, size, and composition of solid-state substrates or colloidal particles, along with the wavelength and intensity of incident light, we can precisely tune the temperature profiles and the resultant thermoelectric fields for versatile particle manipulations.[19−21] It has been demonstrated that colloidal particles can be precisely manipulated in a low-power manner via the optothermoelectric fields that are optically generated either by the optothermal substrates or particles themselves, which are supported by theoretical works on the mechanism of optothermoelectromechanical coupling for colloidal particles.[6,22−24] Thus far, a series of optothermoelectric techniques have been developed to provide versatile particle manipulations.[25−27] Such optothermoelectric tweezers have expanded the tool box for manipulating colloidal particles at the micro- or nanoscale, which also includes tweezers based on diffusiophoresis,[28−30] electric tweezers,[31−33] acoustic tweezers,[34,35] optical tweezers,[15,36,37] optoelectronic tweezers,[17] and other optofluidic techniques.[38,39] Impressively, taking advantage of entropically favorable photon−phonon conversion and universally applicable thermophoretic migration, optothermoelectric tweezers can manipulate colloidal particles of various materials, shapes,

Received: November 2, 2020
Revised: December 16, 2020
Published: January 7, 2021

ACS Publications

© 2021 American Chemical Society

https://dx.doi.org/10.1021/acs.langmuir.0c03182
Langmuir 2021, 37, 1315−1336

and sizes at single-particle resolution with low power and simple optics.[40−44] By exploiting self-generated optothermoelectric fields of light-absorbing particles such as amorphous silicon (a-Si) beads and Janus particles, we have extended optothermoelectric trapping to optical pulling and microswimmers.[45,46]

This Invited Feature Article focuses on the fundamentals and applications of optothermoelectric phenomena in colloidal solutions. We start with an introduction on the fundamentals of optothermoelectrics, including the optothermal effect and thermoelectric effect. Next, we discuss a series of optothermoelectric technologies and their applications with a focus on our recent progress. We conclude the article with an outlook on the future development of optothermoelectrics in colloidal solutions.

FUNDAMENTALS OF OPTOTHERMOELECTRICS

The optothermoelectric phenomenon involves two characteristic energy-conversion processes (i.e., light to heat and heat to electric potential), which are known as the optothermal effect and the thermoelectric effect, respectively. In this section, we introduce the main mechanisms of these two effects and briefly discuss how they interact with the suspended colloidal particles.

OPTOTHERMAL EFFECT

Optothermal management at the microscale and nanoscale plays a significant role in the optothermoelectric manipulation of colloidal particles at high spatial resolution. One of the most effective optical approaches toward localized temperature gradients for single-particle manipulation is the plasmonic thermal effect, which is commonly achieved through resonant laser irradiation of metallic nanostructures.[21] The heating of metallic nanostructures stems from the coupling between their localized surface plasmons and the external electromagnetic waves, which reaches its maximum energy conversion frequency at the localized surface plasmon resonance. Furthermore, the coupling amplifies the frequency of collisions between the conductive electrons and lattice atoms, transforming the laser incidence into heat. This process leads to the creation of a heat flux and the corresponding temperature gradient field in the vicinity of the irradiated metallic nanostructures, which is described by[19,21]

$$\rho C_P \frac{\partial T(\boldsymbol{r})}{\partial t} - \nabla\cdot[\tau \nabla T(\boldsymbol{r})] = Q \tag{1}$$

where ρ, C_P, and τ are the density, specific heat capacity at constant pressure, and thermal conductivity of the corresponding domains, respectively. Q is the volumetric heat generation density which represents a source term that stems from the optical heating of the nanostructures. In other words, Q is nonzero for all plasmonic nanostructures that absorb the laser power (and convert it to heat) and zero for other nonabsorbing media. The first term in eq 1 represents the unsteady term, which measures the rate of temperature change as a function of time. The second term shows the distribution of temperature within the medium. Within plasmonic nanostructures, the metallic components usually have high thermal conductivities, resulting in a uniform temperature, while the solution surrounding the nanostructures usually has a low thermal conductivity, resulting in a nonzero temperature gradient. For an array of discrete plasmonic nanostructures, the temperature within individual nanostructures will be uniform due to the high thermal conductivity. However, there exists a temperature gradient across multiple nanostructures due to the nonuniform irradiation of a laser beam on the array and the low thermal conductivity between nanostructures. For continuous-wave illumination, the time to reach a steady state of temperature fields is within the nanosecond regime, and eq 1 can be simplified to $\nabla\cdot[\tau\nabla T(\mathbf{r})] = -Q$.

Energy term Q can be described by heat power density q via[47]

$$Q = \iiint q \, \mathrm{d}V \tag{2}$$

where $q = \frac{1}{2}Re(\mathbf{J}\cdot\mathbf{E}^*)$ with $\mathbf{J}$ and $\mathbf{E}$ being the electronic current density and electric field inside the metallic nanostructure. Q can also be expressed in terms of the incident intensity of light as[48]

$$Q = \sigma_{abs} I \tag{3}$$

where σ_{abs} is the absorption cross section of the metallic nanostructure. For spherical nanostructures, the explicit expression of σ_{abs} can be deduced on the basis of analytical methods (e.g., Mie theory).[49] For complex nanostructures, it is suitable to perform full-scale numerical simulations to obtain σ_{abs}, energy term Q, and the temperature distribution.[50]

Immobilized Light-Absorbing Substrates. For efficient heat generation and the retention of high temperature and its gradient, the nanostructures as light-to-heat converters must possess a high optothermal conversion efficiency and low thermal conductivity simultaneously.[40,43,45,46] A gold-based thermoplasmonic substrate is a viable candidate due to its ease of fabrication and atmospheric stability. One representative example is the gold nanoislands (AuNIs), which are fabricated by thermally annealing thin films of Au on glass substrates to obtain isolated Au nanoparticles.[51] Their surface plasmon resonance wavelength could be tuned using several parameters such as the annealing temperature, rate of annealing, and thickness of the original Au films to obtain the optimized optothermal conversion efficiency at any required laser wavelength. For the AuNIs with their irregular sizes and shapes, the electromagnetic- and temperature-field distributions at the AuNIs were attained by simulations based on scanning electron micrographs and the experimentally measured light absorption efficiency (Figure 1a).[51,52]

To increase the site specificity of the light-induced temperature gradient field with a narrow spatial distribution, which is required for higher-resolution particle manipulation, rationally designed plasmonic nanostructures with well-confined electromagnetic hotspots can be employed for photon−phonon conversion within small areas beyond the diffraction limit of light. For example, Au nanorods (AuNRs) on glass slides were utilized as light-absorbing substrates for the optical generation of well-defined temperature gradients within nanoscale regimes of the colloidal solutions surrounding the AuNRs (Figure 1b).[40] Moreover, the selective activation of the specific plasmon resonance of an AuNR, namely, transversal and longitudinal resonances, could be achieved through aligning the polarization of incident light perpendicular and parallel to the long axis of the nanorod, respectively. The wavelengths of these two resonances can be tuned by the aspect ratio and size of the nanorod. For example, the maximal light absorption was attained when the incident laser wavelength was at the longitudinal resonance wavelength and its electric field was parallel to the long axis of the nanorod. It is worth noting that the angle between the electric field vector of incident light and the long axis of rods plays an essential role in the efficiency of photon−phonon

https://dx.doi.org/10.1021/acs.langmuir.0c03182
Langmuir 2021, 37, 1315−1336

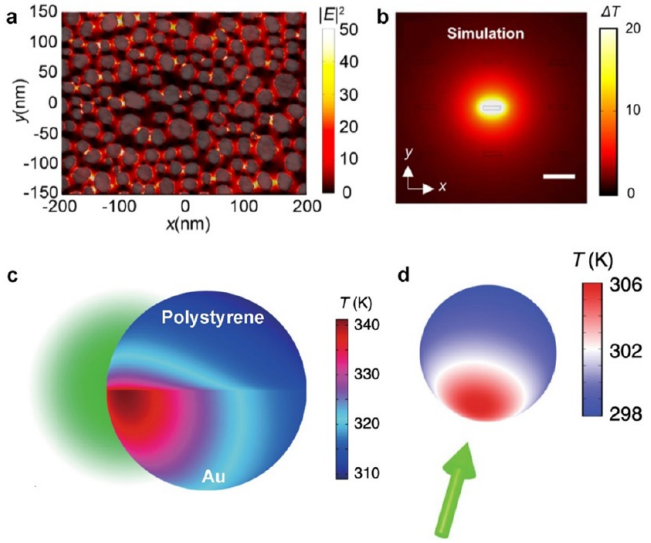

Figure 1. Optothermal effects at representative nanostructures. (a) Simulated electric field of laser-illuminated AuNIs overlaid with their scanning electron micrograph. Adapted with permission from ref 58. Copyright 2017 American Chemical Society. (b) Simulated temperature profile of AuNRs upon illumination with a 780 nm laser beam with a power density of 0.6 mW·μm^{-2}. The scale bar is 1 μm. Adapted with permission from ref 40. Copyright 2018 American Chemical Society. (c) Simulated temperature profile of a 2.7 μm PS/Au Janus particle under off-centered 532 nm laser illumination with the power set at 2 mW. Adapted with permission from ref 46. Copyright 2020 Springer Nature. (d) Simulated temperature distribution of a 700 nm Si particle on a heating laser with an optical power of 60 μW and a beam with a diameter of 2 μm at the focal plane. Adapted with permission from ref 45. Copyright 2020 Springer Nature.

conversion.[53] Therefore, by optimizing the polarization of incident light relative to the AuNR orientation, one can change the trapping stiffness of colloidal particles by the optothermoelectric field around the nanorod.[40]

Suspended Light-Absorbing Particles. Photon−phonon conversion can also be achieved in the light-absorbing particles suspended in solvents, which can generate the optothermoelectric field around the particles under certain conditions. One representative example is the Janus particles that are made of polystyrene (PS) or silica beads with half-coated Au caps (Figure 1c). Bickel et al. investigated the temperature field of heated Janus particles with different thicknesses of Au caps.[54] Let us consider a Janus particle with radius a, thermal conductivity τ_{in} for the pristine part, and thermal conductivity τ_c for the metallic cap of thickness d that is dispersed in solution with thermal conductivity τ_{out}. Since thermal conductivities τ_{in} and τ_{out} meet $\tau_{in} = \tau_{out} = \tau \ll \tau_c$ for most cases, the temperature distribution of the Janus particle can be divided into two typical conditions:

(1) $\tau_c d \ll \tau a$: the temperature field distorted by the metallic cap is neglected.[55] The temperature difference across the sides of the Janus particle is expressed as $\Delta T = \frac{3\epsilon I a}{2(\tau_{out} + \tau_{in})}$, where ϵ is the absorption efficiency of the metallic cap and I is the laser intensity.

(2) $\tau_c d \gg \tau a$: the metallic cap is assumed to have a constant temperature, and the temperature field is given as $T(a, \theta) = T_0 + \Delta T$.[54]

The self-generated temperature gradient of the Janus particle along with its asymmetry can induce the motion effects of the particle such as swimming and rotation under laser illumination.[46]

Some pristine dielectric micro- or nanoparticles such as a-Si beads can also have a high optothermal conversion efficiency with low thermal conductivity.[56] Unlike Janus particles whose temperature field direction is determined geometrically, the direction of the temperature gradient for optically heated a-Si beads depends only on the incident direction of light (Figure 1d).[57] Therefore, the direction of resultant thermoelectric fields can be manipulated by the incident light. The a-Si beads cannot be manipulated only by their self-generated optothermoelectric field but also can serve as mobile optothermal substrates to trap and transport other colloidal particles.[45]

THERMOELECTRIC EFFECT

The thermoelectric effect describes the establishment of an electric potential under a temperature gradient. In this section, we will start with a brief introduction to thermophoresis, which is at the core of the thermoelectric effect in electrolyte solutions. Next, we summarize the basics of the thermoelectric effect in electrolyte solutions. Readers are referred to an excellent review article by Würger for more details.[5] Finally, we discuss recent progress in elucidating how the thermoelectric field and its interplay with colloidal particles depend on the solvent properties, solute properties, and temperature.

Thermophoresis. Thermophoresis (also known as thermodiffusion, thermal diffusion, or the Soret effect) describes the directed motion of suspended particles, molecules, droplets, or micelles in a complex fluid under a temperature gradient of ∇T.[59] The drift velocity is given by

$$\mathbf{u} = -D_T \nabla T \tag{4}$$

where D_T represents the thermophoretic mobility or thermal diffusion coefficient. When a dilute fluid reaches a steady state under a temperature gradient, the concentration gradient of suspended objects is expressed as $\nabla c = -cS_T \nabla T$.[11] $S_T = D_T/D$ is called the Soret coefficient, with D being the Einstein coefficient or Brownian diffusion coefficient. Accordingly, under a temperature gradient, solute particles that move toward the cold region ($S_T > 0$) are termed thermophobic particles, while solute particles that move toward the hot region ($S_T < 0$) are called thermophilic particles.

Fundamentals of the Thermoelectric Effect in a Basic Version. It has been observed that the sign of D_T can be altered by changing the ambient temperature or salinity of colloidal solutions.[1,2] For example, the Soret coefficients of lysozyme proteins,[60,61] polystyrene beads,[1,11,61,62] micelles,[62] DNAs,[63] and Ludox particles in solutions[64] exhibited similar temperature dependences.[60] At low ambient temperatures, these solutes were thermophilic under a temperature gradient field, resulting in movement toward the hot region. As the temperature exceeded a critical temperature T^*, the sign of D_T was reversed, leading to thermophobic behavior. In another example, the D_T of PS beads in a buffered electrolyte solution changed from negative to positive values upon addition of a salt such as NaCl or LiCl to the solution.[2] The change was attributed to the fact that the differential movement of ions in these salt solutions generated a thermoelectric field, which interacted with the PS beads. This indicates that the thermoelectric effect can play a critical role in the thermophoretic motion of solutes in electrolyte solutions.

When a temperature gradient is applied to an electrolyte solution, the anions and cations can drift along the thermal

https://dx.doi.org/10.1021/acs.langmuir.0c03182
Langmuir 2021, 37, 1315−1336

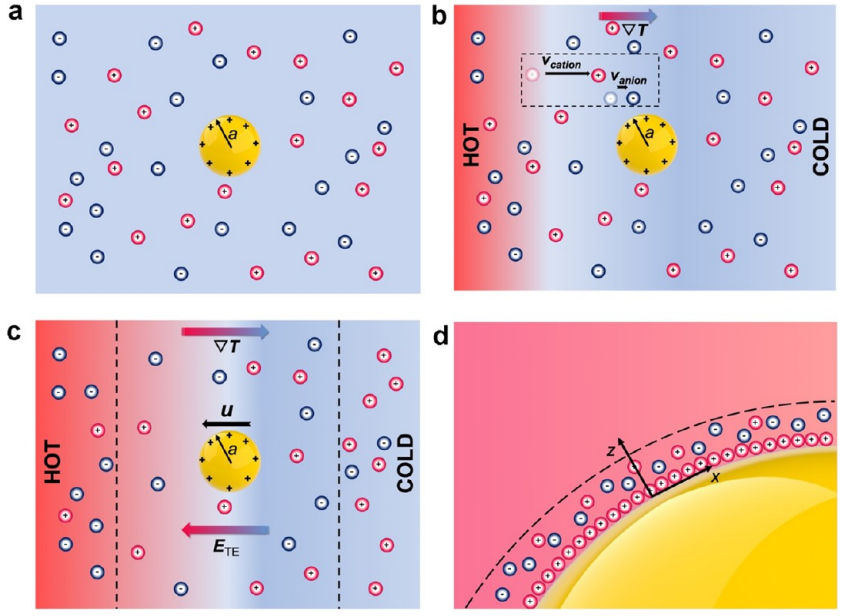

Figure 2. Schematic of the formation of a thermoelectric field in a closed colloidal system under a one-dimensional constant temperature gradient. (a) Original state without a temperature gradient. (b) Onset of ionic redistribution under ∇T. The drift velocity of cations (v_{cation}) is larger than that of anions (v_{anion}) in this schematic. The relationship between v_{cation} and v_{anion} can change with the type of cations and anions. (c) Steady state of the thermoelectric field. ∇T, $\mathbf{E}_{TE}$, and $\mathbf{u}$ represent the external temperature gradient, thermoelectric field, and particle velocity, respectively. The particle with radius of a is positively charged. Circles with positive and negative signs indicate ions with positive and negative charges. (d) Magnified view of the particle surface when the particle radius a is significantly larger than the Debye length λ (i.e., the distance between the dashed line and the particle surface; the distance to the real case is much smaller than that shown here). The z axis is defined to be perpendicular to the particle surface.

gradient with different speeds or even in opposite directions, which is determined by their size and solvent energy (Figure 2a,b).[65] Considering an electrolyte with monovalent ions of charge $q_i = Z_i e$ ($Z_i = \pm 1$) and densities n_i, the thermophoretic motions of different ions lead to ion currents, each of which can be given by[5,65−67]

$$\mathbf{J}_i = -D_i\left(\nabla n_i + n_i\frac{Q_i^*}{k_B T^2}\nabla T - n_i\frac{q_i\mathbf{E}_\infty}{k_B T}\right) \tag{5}$$

where D_i is the diffusion coefficient defined as $D_i = k_B T/6\pi\eta a_i$ (a_i is the radius of the ion and η is the viscosity of the surrounding medium), Q_i^* is the ionic heat of transport, $\mathbf{E}_\infty$ is the net electrical field (any external electric field along with the thermoelectric field), and k_B is the Boltzmann constant. The three diffusion terms depend on a concentration gradient (osmosis), a thermal gradient (thermophoresis), and an electric field (electrophoresis), respectively.

When the ionic redistribution reaches a steady state for a closed system with solid boundaries and without external forces acting on the ions, the ion currents vanish: $\mathbf{J}_i = 0$ (Figure 2c). Since different ions commonly have different Soret coefficients, cations and anions have diverse concentration profiles, which leads to a corresponding charge density $\rho_\infty = \sum_i q_i n_i$ that is proven to be negligible in the system for temperature gradients of up to 1−10 K/μm.[65,66] Under the higher temperature gradients, ions physically separate as observed from molecular dynamics (MD) simulations.[68,69] The salinity gradient is given by[5]

$$\frac{\nabla n_0}{n_0} = -\alpha\frac{\nabla T}{T} \tag{6}$$

where n_0, namely, the salinity, is defined as $n_0 = \frac{1}{2}\sum_i n_i$. α is the reduced Soret coefficient of the electrolyte solution, which is expressed as

$$\alpha = \sum_i \alpha_i\frac{n_i}{n_0},\ \alpha_i = \frac{Q_i^*}{2k_B T} \tag{7}$$

In addition, the Soret coefficient, S_T, can be correlated with the reduced Soret coefficient α_i through $S_T = \sum_i\alpha_i/T$. Furthermore, considering $\sum_i J_i = 0$ and $\rho_\infty = \sum_i q_i n_i = 0$, the thermoelectric field $\mathbf{E}_{TE}$ can be obtained:[70,71]

$$\mathbf{E}_{TE} = S\nabla T = \delta\alpha\frac{k_B\nabla T}{e} = \frac{k_B T\nabla T}{e}\frac{\sum_i Z_i n_i S_{Ti}}{\sum_i Z_i^2 n_i} \tag{8}$$

where S is the Seebeck coefficient and Z_i is the charge number with $Z_i = \pm 1$ for positive and negative monovalent ions. The dimensionless coefficient $\delta\alpha$ is expressed as

$$\delta\alpha = \sum_i Z_i\alpha_i\frac{n_i}{n_0} \tag{9}$$

It has been reported that the time for the formation of thermoelectric fields via heating a single particle is on the time scale of the thermal diffusion of salt ions over one Debye length, which is on the order of microseconds and can be negligible during the colloidal analysis.[6] Meanwhile, a steady concentration profile of salt solutions under a one-dimensional temperature gradient, where the finite temperature difference is set across a width w, can be achieved on a time scale of $\tau \cong w^2/(\pi^2 D)$, where D is the Brownian diffusion coefficient.[72] For a typical laser heating scenario, w can be treated as 1 μm, and the obtained time scale is on the order of microseconds.

After obtaining a common expression for the thermoelectric field, let us consider how solutes such as colloidal particles are

https://dx.doi.org/10.1021/acs.langmuir.0c03182
Langmuir 2021, 37, 1315−1336

transported in electrolyte solutions under temperature gradients.[73] The relevant microfluid is usually described on the basis of the Navier−Stokes' equation

$$\eta\nabla^2 v = \nabla P - \mathbf{f} \tag{10}$$

where η is the viscosity of the fluid, P is the hydrostatic pressure, and $\mathbf{f}$ is the force density on the fluid applied by a neighboring suspended particle. Considering a suspended particle with radius a that is significantly larger than the Debye length (Figure 2d), the boundary-layer approximation is valid, for which the particle surface can be regarded to be flat during force analysis.[74] Thus, the velocity perpendicular to the particle is zero $v_z = 0$, while the velocity parallel to the surface v_B and the transport velocity of a suspended particle $\mathbf{u}$ are given by[5,74]

$$v_B = \frac{1}{\eta}\int_0^B \mathrm{d}z\, z\left(f_x - \frac{\mathrm{d}P}{\mathrm{d}x}\right),\ \mathbf{u} = -\frac{2}{3}\overline{v}_B \tag{11}$$

where B is upper limit of the range of the force field, f_x is the parallel component of force density exerted on the particle, and $\overline{v}_B$ is the boundary velocity of the particle.

In order to solve the integral of v_B in eq 11 and attain the transport velocity $\mathbf{u}$ and the Soret coefficient D_T, the force density $\mathbf{f}$ can be further given by a charge term and a dielectric term[2,75]

$$\mathbf{f} = \rho\overline{\mathbf{E}}_\mathbf{0} - \rho\nabla\boldsymbol{\psi} - \frac{1}{2}\mathbf{E}^2\nabla\varepsilon \tag{12}$$

where ρ is the charge density ($\overline{E}_0$ is the macroscopic (external) electric field, $\boldsymbol{\psi}$ represents the electrostatic potential, $-\nabla\boldsymbol{\psi}$ is interpreted as the localized electric field due to ionic redistribution within the Debye layer, $\boldsymbol{E}$ is the electric field of the charged particle, and $\nabla\varepsilon$ is the gradient of the medium's permittivity. In addition, the hydrostatic pressure P increases due to the excess ion density in the electric double layer around the charged suspended particle.[76] The excess ion densities of different ions are given by $\delta n_i = n_i(e^{-Z_i e\psi/k_BT} - 1)$ based on the Poisson−Boltzmann theory, by which the local charge density is given as $\rho = -2en_0\sinh(e\psi/k_BT)$ while the excess ion density n is demonstrated to be $n = 2n_0\,(\cosh(e\psi/k_BT) - 1)$, where n_0 is bulk salinity.[2] Since $P = P_0 + nk_BT$, where P_0 is the hydrostatic pressure far away from the particle, the gradient of the hydrostatic pressure, along with interdependencies of n and T, is[5]

$$\nabla P = -\rho\nabla\psi + (\rho\psi + nk_B T)\frac{\nabla T}{T} + nk_B T\frac{\nabla n_0}{n_0} \tag{13}$$

When the permittivity of the solvent is significantly larger than that of the particle ($\varepsilon_{solvent} \gg \varepsilon_{particle}$) and the thermal conductivity of the solvent is approximately equal to that of the particle ($\tau_{solvent} \approx \tau_{particle}$, for which most particle materials satisfy except for metals), the transport velocity can be deduced by combining eqs 11−13[5]

$$\mathbf{u} = -\frac{\varepsilon(\zeta^2 - 3\zeta_T{}^2)}{3\eta}\frac{\nabla T}{T} + \frac{\varepsilon\zeta_T{}^2}{3\eta}\left(\frac{\nabla\varepsilon}{\varepsilon} + \frac{\nabla n_0}{n_0}\right) + \frac{\varepsilon\zeta}{\eta}\mathbf{E}_0 \tag{14}$$

where ε, η, and n_0 are the permittivity, viscosity, and salinity of the solvent, respectively. Meanwhile, the surface potential ζ can be given as $\zeta = \frac{2k_BT}{e}\mathrm{arcsinh}(2\pi\sigma l_B\lambda)$ where σ is the number density of element charges, l_B is the Bjerrum length ($l_B = e^2/4\pi\varepsilon k_BT_0$), and λ is the Debye length; ζ_T is a defined parameter that is related to ζ and T ($\zeta_T{}^2 = \left(\frac{2k_BT}{e}\right)^2 2\ln\cosh\frac{e\zeta}{4k_BT}$). When eqs 4 and 14 were combined, a general expression for the thermophoretic mobility is given by[5]

$$D_T = \frac{\varepsilon}{\eta T}\left(\frac{\zeta^2}{3} + \zeta\psi_0 - \zeta_T{}^2\left(1 - \frac{\alpha+\tau}{3}\right)\right) \tag{15}$$

where α is defined by eq 7 and corresponds to the salinity gradient and τ is related to the permittivity gradient that is defined as $\frac{\nabla\varepsilon}{\varepsilon} = -\tau\frac{\nabla T}{T}$.[77] For weakly charged particles ($e\psi \ll k_BT$), ζ_T can be equal to $\frac{1}{2}\zeta$ based on the Debye—Hückel approximation.[5,78] However, for highly charged particles, the Debye−Hückel approximation ceases to be valid, and $\zeta_T{}^2$ is negligible.[79] The thermophoretic mobility is then transformed to[70]

$$D_T = \frac{\varepsilon}{\eta T}\left(\frac{\zeta^2}{3} + \zeta\psi_0\right) = \frac{\varepsilon\zeta^2}{3\eta T} - \frac{\varepsilon\zeta}{\eta}S \tag{16}$$

The first term is related to the thermo-osmotic flow,[80,81] which is always positive and drives the suspended particle to the cold region. On the contrary, the second term related to the electric field can take both signs. Overall, the Soret coefficient of solutes in electrolyte solutions can be either positive or negative, which implies that the suspended particles can migrate to the cold or the hot region depending on the solvents' and particles' properties.

It is worth noting that although the above discussion gives us a basic picture of the thermoelectricity it was derived on the basis of a single colloidal sphere in a dilute electrolyte solution with a one-dimensional constant temperature gradient. Several other parameters, including the solvent properties, solute properties, collective effects, and temperature profile distortion, can influence the thermoelectric effect, which will be discussed more thoroughly in the next subsections.

Dependence of the Thermoelectric Effect on Solvent Properties. It has been established that the electrolyte composition affects the thermophoretic mobility D_T of charged colloidal particles.[1] As shown in Table 1,[2] the negatively charged

Table 1. Heat of Transport Q_i^*[84] and Reduced Soret Coefficient α_i of Six Ions in Dilute Systems at Room Temperature[a]

ion	H^+	Li^+	K^+	Na^+	OH^-	Cl^-
Q_i^*(kJ/M)	13.3	0.53	2.59	3.46	17.2	0.53
α_i	2.7	0.1	0.5	0.7	3.4	0.1

[a]Adapted with permission from ref 2. Copyright 2008 American Physical Society.

PS beads in a cyclohexyl-3-aminopropanesulfonic acid-buffered electrolyte solution (pH 10.5) originally drifted toward the warm region due to the large α (i.e., reduced Soret coefficient) of OH^- ions. However, the effect of OH^- ions on the Seebeck coefficient $S = \frac{k_B}{e}\delta\alpha$ was weakened by the addition of NaCl or LiCl that contained $Na^+/Li^+/Cl^-$ ions with small α. The addition of these ions caused a reversal in the D_T of the PS beads and drove the beads toward the cold region. In addition, the α values of H^+ and OH^- ions are significantly higher than those of the other ions, which indicates that the pH value and protonated buffers play a key role in the thermoelectric effect.[1,2,61,62,82] On

https://dx.doi.org/10.1021/acs.langmuir.0c03182
Langmuir 2021, 37, 1315−1336

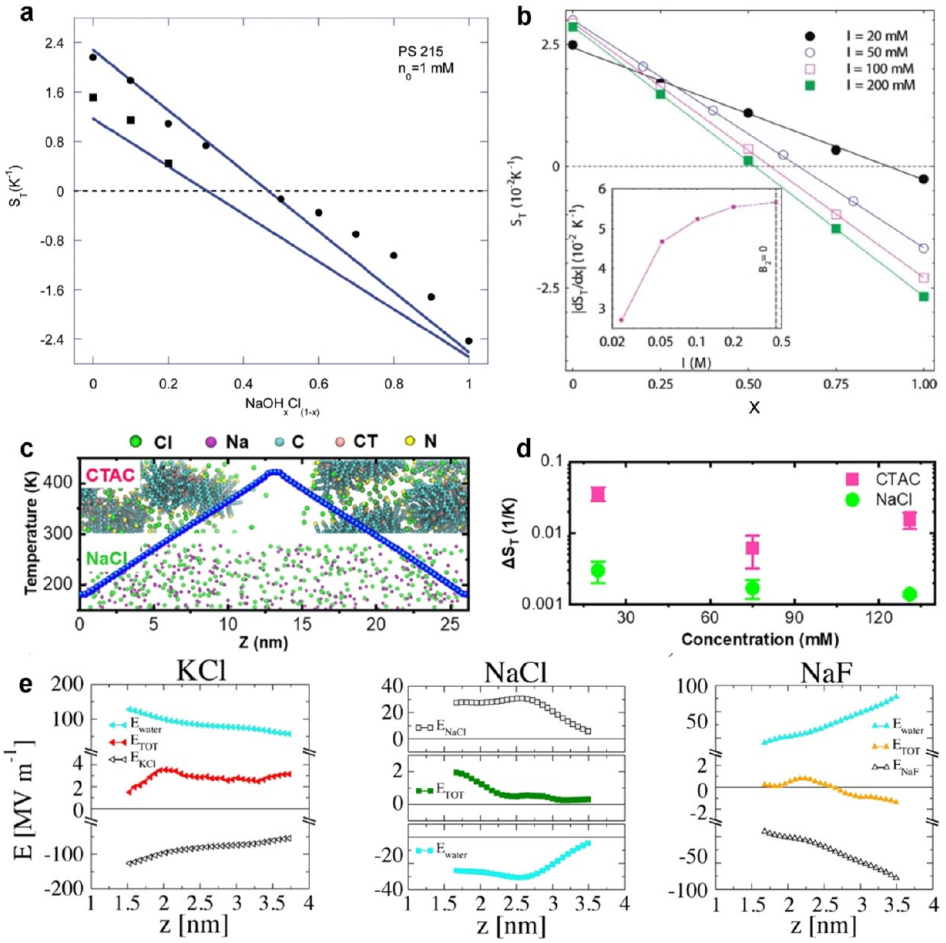

Figure 3. Dependence of the Soret effect of colloidal particles on electrolyte ions. (a) Soret coefficient of 215 nm PS beads in ternary electrolyte $NaOH_xCl_{(1-x)}$. The square and circle data were measured at 26 and 41 °C, respectively. The solid line was calculated on the basis of $S_T = \frac{6\pi a}{k_B T^2}\left(\frac{\varepsilon\zeta^2}{12}(1 + \tau + \alpha) - \varepsilon\zeta ST\right)$. Adapted with permission from ref 4. Copyright 2014 Royal Society and Chemistry. (b) The Soret coefficient of SDS micelles in a $NaCl_{1-x}OH_x$ solution changed as a function of the molar fraction x of NaOH. Four curves correspond to four different ion strengths. Adapted with permission from ref 3. Copyright 2010 American Chemical Society. (c) Molecular dynamics simulations show the ion distribution of CTAC and NaCl at steady state (concentration = 1 M). The blue dotted line represents the temperature profile. (d) Soret coefficient difference between cations and anions of CTAC and NaCl. Adapted with permission from ref 24. Copyright 2020 Springer. (e) Water-polarization-induced, ion-separation-induced, and total electric fields of 1 M·kg^{-1} KCl (left), NaCl (middle), and NaF (right) aqueous solutions under a temperature gradient like that in (c). Adapted with permission from ref 69. Copyright 2018 American Chemical Society.

the basis of this understanding, Vigolo et al. exploited a microfluidic device with an applied external temperature gradient to prove that 477 nm PS beads exhibited different drift directions upon changing the electrolyte from NaOH to NaCl.[72] Eslahian et al. further demonstrated the change in Soret coefficients of 215 nm PS beads in ternary electrolyte $NaOH_xCl_{(1-x)}$ (Figure 3a).[4] Furthermore, it was observed that sodium dodecyl sulfate (SDS) micelles altered the sign of S_T in a $NaCl_{1-x}OH_x$ solution upon varying the proportion of OH^- ions (Figure 3b).[3]

Recently, Ding et al. have performed MD simulations to explore the Soret coefficient S_T of different ions on the atomic scale.[24] The simulations revealed that different ions showed distinctive steady-state distributions under extremely high temperature gradients of 1−10 K/nm, a prerequisite for MD simulations (Figure 3c). The atomic distributions were used to calculate their S_T values based on equation $S_T = -1/x(dx/dT)$, where x is the molar fraction of the solute. As shown in Figure 3d, ΔS_T ($\Delta S_T = S_T(\text{cation}) - S_T(\text{anion})$) values of different electrolyte solutions also have diverse ion strength dependences,[67] which can be explained by the effective Soret coefficient of an ion:[65]

$$S_T = S_T^* + \Delta S_T^{\text{coupling}} = S_T^* - \frac{Z_i \sum Z_i C_i S_{Ti}^*}{\sum C_i} \quad (17)$$

where S_T^* is the intrinsic ionic Soret coefficient, $\Delta S_T^{\text{coupling}}$ is the Soret coefficient change due to charge coupling, and Z_i and C_i are the sign and concentration of ion i, respectively. Since $S_T^*(Na^+) > S_T^*(Cl^-)$, $\Delta S_T^{\text{coupling}}$ is negative and its magnitude increases when the ionic concentration increases. Thus, a monotonic decrease in ΔS_T with respect to NaCl is obtained. For cetyltrimethylammonium chloride (CTAC) solutions, the decrease in ΔS_T is attributed to the same reason as for NaCl, while the increase in ΔS_T above 75 mM stems from the fast increase in $S_T(CTA^+)$. Specifically, since larger polymer molecules tend to have higher S_T, an increase in the concentration leads to a larger size of CTA^+ micelles, which promotes $S_T(CTA^+)$ and further increases ΔS_T. The thermoelectric field can also arise from the polarization of water

https://dx.doi.org/10.1021/acs.langmuir.0c03182
Langmuir 2021, 37, 1315−1336

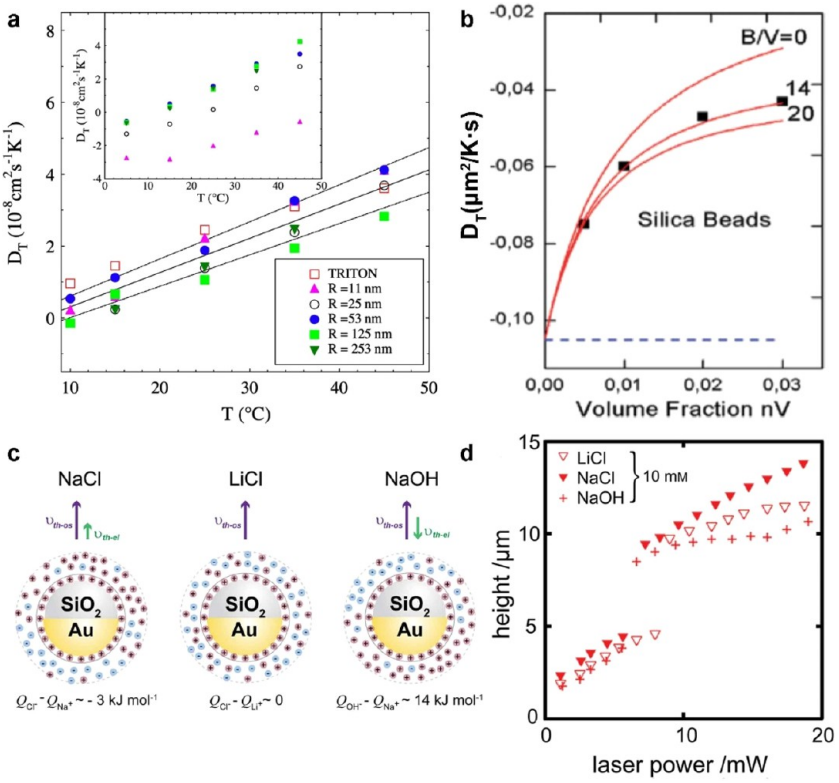

Figure 4. (a) Thermophoretic mobility of Triton-coated PS particles with different sizes and temperatures (ionic strength = 10 mM). Adapted with permission from ref 11. Copyright 2008 American Physical Society. (b) Volume fraction (or concentration) dependence of D_T of 70 nm silica beads in a sulfo-rhodamine B solution (30 μM/L). The point data are from ref 87, and the curves are calculated on the basis of eq 21. Adapted with permission from ref 13. Copyright 2011 American Physical Society. (c) Schematic represents the motion of Janus particles in different electrolyte solutions. v_{th-os} and v_{th-el} are the thermo-osmotic and thermoelectric velocities, respectively. Q represents the heat of transport of different ions. (d) Axial displacement of optically trapped Janus particles in different electrolyte solutions as a function of laser power. Adapted with permission from ref 93. Copyright 2016 Wiley-VCH.

molecules in solutions. Relevant studies based on MD simulations revealed that both water polarization and charge separation play a significant role in the formation of thermoelectric fields ($E_{tot} = E_{ions} + E_{water}$) in aqueous solutions under temperature gradients.[68,69,83] The simulation results showed that water polarization induces diverse thermoelectric fields in different salt solutions (Figure 3e), implying the existence of intricate water−ion coupling mechanisms. By comparing the simulated results of Seebeck coefficients with the values obtained from the equation $S = \frac{(Q_+^* - Q_-^*)}{2eT}$, where Q_+^* and Q_-^* are the ionic heat of transport, one concludes that this equation is suitable only for dilute solutions, noting that this equation may be invalid for concentrated solutions due to the lack of consideration of ion−ion interactions.[69]

It is important to mention that the dissolved electrolyte can also be exploited to change the surface charge of suspended colloidal particles. For example, CTAC can be attached to a particle to form a positively charged surface regardless of its original surface charge.[43] This surface charge modification can significantly change the thermophoretic mobility of the particle under a temperature gradient.

Dependence of the Thermoelectric Effect on Particle Properties. Our simplified discussion on the basics of the thermoelectric effect in Section 4 is based on dilute pristine spherical particles that have a radius significantly larger than the Debye length ($a \gg \lambda$). Herein, we briefly discuss how the particle size, particle concentration (which is relevant to collective effects), and particle composition (e.g., Janus particles) influence the thermoelectric effect.

Particle Size. In Section 4, the drift velocity and thermophoretic mobility D_T of particles with $a \gg \lambda$ are given by eqs 14 and 15 based on the boundary layer approximation. However, extremely weak electrolyte solutions or small particles (e.g., molecular ions) can lead to the opposite situation, where $a \ll \lambda$ and the Hückel limit should be applied. Morthomas et al. compared these two conditions quantitatively:[12]

$$D_T = \frac{\varepsilon}{3\eta T}\left(\zeta^2\tau - 2\zeta\frac{k_B T}{e}\delta\alpha\right) (a \ll \lambda) \quad (18)$$

$$D_T = \frac{\varepsilon}{3\eta T}\left(\zeta^2\frac{\tau + \alpha + 1}{4} - 3\zeta\frac{k_B T}{e}\delta\alpha\right) (a \gg \lambda) \quad (19)$$

It is observed that the components are similar in both cases, but a factor of $^3/_2$ is added to the Seebeck effect term of eq 19 compared with eq 18. This is due to the permittivity variation around the particle with $a \gg \lambda$, where $E_{T,\|}$ is enhanced by the permittivity contrast via $3\varepsilon_{liquid}/(2\varepsilon_{liquid} + \varepsilon_{particle}) \approx {}^3/_2$ due to common $\varepsilon_{liquid} \gg \varepsilon_{particle}$.[12] However, the permittivity difference along with the thermal conductivity discontinuity is neglected for the $a \ll \lambda$ condition, which loses the factor of $^3/_2$.[12]

Moreover, the thermophoretic mobility D_T of large particles has been found ($a \gg \lambda$ is independent of the particle size a, while the D_T of particles with $a \ll \lambda$ is dependent on the particle size (Figure 4a)).[2,11,74] This result stems from the surface potential

https://dx.doi.org/10.1021/acs.langmuir.0c03182
Langmuir 2021, 37, 1315−1336

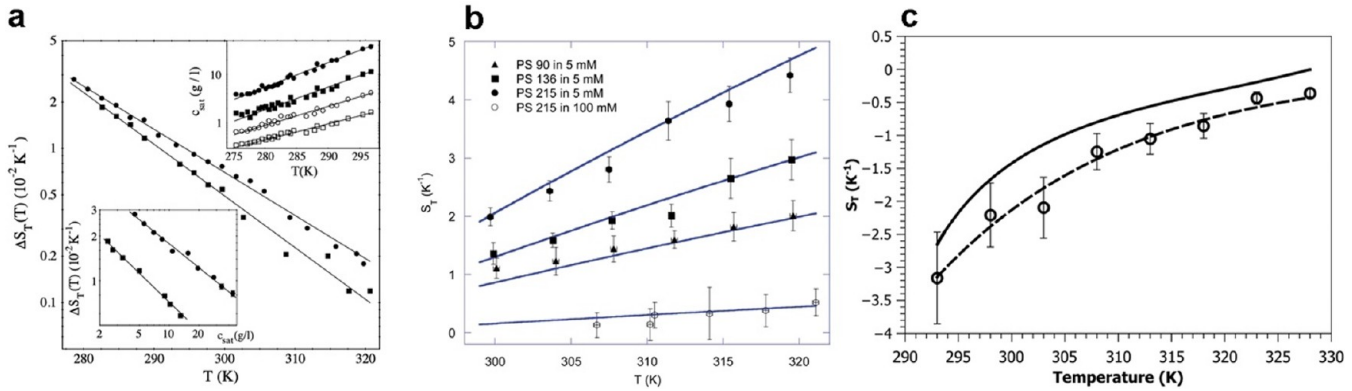

Figure 5. Temperature influence on the electrolyte Soret effect. (a) Relationship between $\Delta S_T(T) = |S_T(T) - S_T^{\infty}|$ and the temperature of the lysozyme. The upper-right inset indicates the solubility of lysozyme solutions at pH 4.65 in equilibrium with tetragonal crystals.[97] The lower left-inset shows the jointed plot of the main set, and the upper-right inset is in a common T range. Different symbols indicate that experiments were performed in the presence of 2 (●), 3 (■), 4 (○), and 5% (□) added NaCl. Adapted with permission from ref 60. Copyright 2003 IOPscience. (b) Temperature dependence of the Soret coefficient of PS beads in NaCl solutions arising from the Seebeck coefficient, S, and the reduced Soret coefficient, α. Adapted with permission from ref 4. Copyright 2014 The Royal Society of Chemistry. (c) Temperature dependence of the Soret coefficient of suspended magnetic colloids. The solid curve is calculated by modifying eq 23: $S_T = S_T^{CM} + S_T^{EL}$; the dashed curve is calculated on the basis of eq 22. Adapted with permission from ref 10. Copyright 2015 American Physical Society.

based on the Debye—Hückel approximation, $\zeta = \frac{\sigma e}{\varepsilon}\frac{a\lambda}{a+\lambda}$, which can be simplified to $\zeta = ae\sigma/\varepsilon$ and $\zeta = \lambda e\sigma/\varepsilon$ when $a \ll \lambda$ and $a \gg \lambda$, respectively. Accordingly, eq 18 is transformed into a linear relationship between D_T and the particle radius when $a \ll \lambda$, while D_T is related to the Debye length rather than the particle size if $a \gg \lambda$. Furthermore, the interfacial properties of colloidal particles can also deviate from the relationship between D_T and particle size. The size independence of D_T for $a \gg \lambda$ ceases to be valid when the colloidal particles have nonwetting surfaces, where the slip boundary condition (i.e., hydrodynamic slippage) takes effect at the liquid−particle interfaces.[85]

Particle Concentration. Several studies have validated that when the solute concentration increases, the interaction among suspended particles could lead to collective effects and influence the electrolyte Seebeck effect and related parameters (e.g., $\mathbf{E}_0$, D_T, and S_T).[3,8,13,14,86−90] Majee et al. have developed a theoretical framework for the collective effects of charged colloids to explain the experimental findings (Figure 4b).[13] Considering negatively charged particles with a concentration n in an electrolyte solution of ion strength n_0 under a one-dimensional constant temperature gradient, the thermoelectric field and thermophoretic mobility are given as[13]

$$\mathbf{E}_0 = -\frac{2(1+\phi)\alpha_+ - 2\alpha_- - \phi T\mu_T/D}{2+\phi+\phi\xi}\frac{k_B\nabla T}{e} \tag{20}$$

$$D_T = \frac{D_T^0}{1+\frac{\phi}{2+\phi}\xi} \tag{21}$$

where μ_T is the thermodiffusive mobility solely related to the phoretic transport velocity. ϕ and ξ are two parameters defined as $\phi = \frac{Z\bar{n}}{n_0}$ and $\xi = \frac{k_BT}{e}\frac{|\mu|}{D}$, where Z and $\bar{n}$ are the valency and average concentration of solutes and μ is the colloidal electrophoretic mobility. For dilute solutions where $\phi \to 0$, the eq 20 is simplified to eq 8, indicating no collective effects in dilute particle solutions. Moreover, the collective effects proceed where $\frac{1}{2}\phi\xi \approx 1$. Since the value of ϕ is usually ∼0.1, ξ is estimated to be ∼20 for suspended particles with collective effects. The ξ of particle sizes between 10 and 10^3 nm is generally in the range of 10 to 10^3, meaning that the collective effects are widely applicable to various concentrated colloidal systems.

Particle Composition. We highlight Janus particles as an example of the dependence of the thermoelectric effect on particle composition. Janus particles are a particular classification of solutes with two or more different physical properties on single particles. The most widely studied Janus particles are dielectric beads with half-coated metallic caps.[55] These particles have heterogeneous light absorptivity, permittivity, and thermal conductivity. Thus, the electrolyte Seebeck effect is supposed to be modified for Janus particles.[22,91,92]

Upon light illumination, a temperature gradient is formed around the Janus particle, directed from the metallic cap to the dielectric part. A thermoelectric field is then established by the ionic redistribution along the thermal gradient. Ly et al. found that although the electric fields close to the surface of the metallic cap and counterpart were quite different due to distinctive electrical conductivity, the slip velocity remained the same for both sides of the particle.[22] Specifically, since there is a polarization charge existing on the metallic cap, the parallel electric field is given as $E_{\parallel}(z) = S\nabla_{\parallel}T_S(1 - e^{-z/\lambda})$ for the conductive surface. Correspondingly, the electric field of the counterpart (i.e., a charged dielectric surface) is given as $E_{\parallel}(z) = S\nabla_{\parallel}T_S - \nabla_{\parallel}\varphi_{\sigma l}$, where the second term is usually negligible. However, the slip velocity is identical across the Janus particle regardless of the materials[22,92] and is given as $\mathbf{u} = -\langle(1 - \mathbf{nn})\cdot\mathbf{v}_B\rangle$ ($\mathbf{v}_B$ is given in eq 11). Additionally, the temperature gradient from the thermal conductivity contrast of different materials can be neglected when the thickness of the metallic cap is less than 10 nm,[54] which is suitable for most recent experiments. Simoncelli et al. have exploited the thermoelectric effect to tune the motion of Janus particles experimentally.[93] By alternating the salt types, NaCl, LiCl, and NaOH, the sign and amplitude of the drift velocity were altered due to the variation of the thermoelectric effect (Figure 4c). Accordingly, the axial displacement of optically trapped Janus particles could be changed by switching the salt type (Figure 4d). However, the data do not provide a conclusive explanation of the thermoelectric field driven along the metallic cap.

https://dx.doi.org/10.1021/acs.langmuir.0c03182
Langmuir 2021, 37, 1315−1336

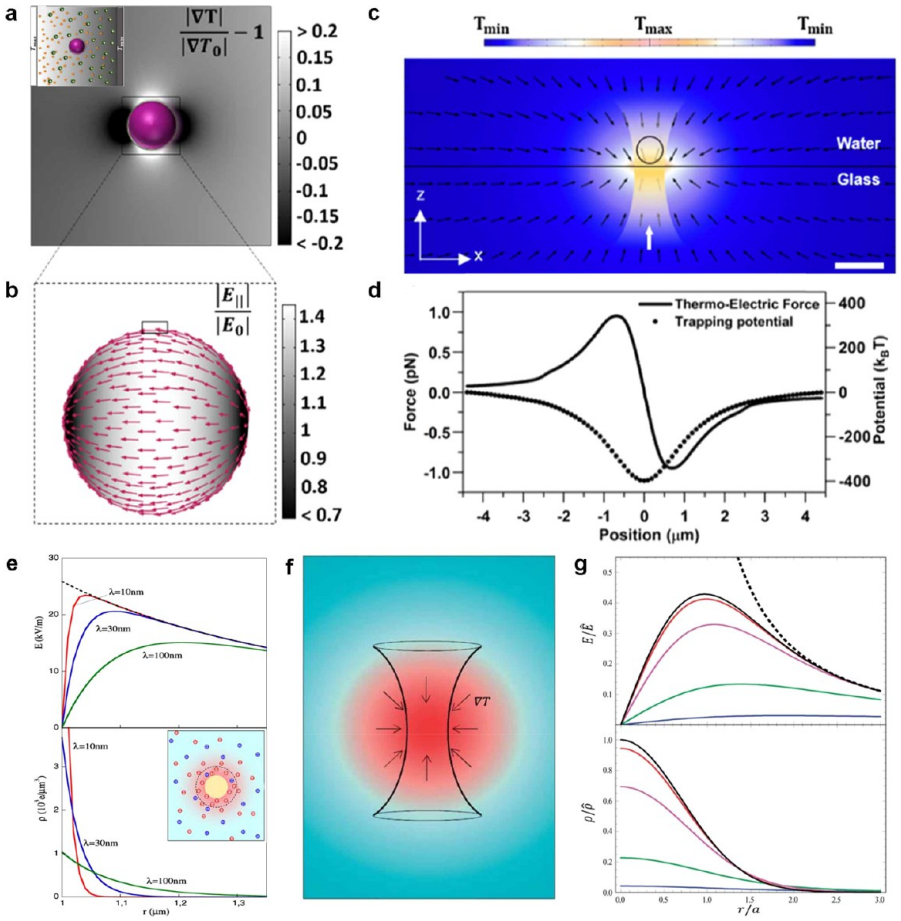

Figure 6. Electrolyte Seebeck effect under different temperature profiles. (a) One-dimensional temperature field distorted by a PS bead. The inset shows the thermoelectric field of a constant-temperature gradient. (b) Ratio of the effective tangential electric component $E_{T,\|}$ and bulk thermoelectric field E_0 at the PS bead. (c) Schematic shows the temperature profile when a single PS particle is on a thermoplasmonic substrate at the interface of water and glass upon laser illumination. Black arrows indicate temperature gradient vectors, and a white arrow indicates the laser propagation direction. The scale bar is 1 μm. (d) Thermoelectric force and trapping potential acting on the PS bead as a function of position. Adapted with permission from ref 23. Copyright 2019 American Chemical Society. (e) Thermoelectric field (upper) and charge density (lower) as a function of distance r and different Debye lengths with particle radius $a = 1$ μm. The inset shows the ionic distribution induced by a heated particle. Adapted with permission from ref 6. Copyright 2012 American Physical Society. (f) Schematic of a localized heated volume in an electrolyte solution irradiated by a focused laser beam. (g) Thermoelectric field (upper) and charge density (lower) as a function of r/a. The solid curve is calculated by a Gaussian heating profile, and the dashed line indicates the electric field based on a point charge. Adapted with permission from ref 70. Copyright 2013 The Royal Society of Chemistry.

Dependence of the Thermoelectric Effect on Temperature. Soret effects of various solutes have similar temperature dependences, which can be well described by an equation proposed by Piazza and colleagues[60]

$$S_T(T) = S_T^{\infty}\left[1 - \exp\left(\frac{T^* - T}{T_0}\right)\right] \tag{22}$$

where S_T^{∞}, T^*, and T_0 represent the high-temperature limit of the Soret coefficient, the critical temperature, and the strength of the temperature effects, respectively. However, the underlying mechanism for this empirical formula is still unclear. Before eq 22 was proposed, some studies revealed that the coefficients α of some salts such as NaCl and KCl were proportional to temperature.[94,95] Subsequently, the relationship between coefficient $\delta\alpha$ and T for charged PS beads in the NaCl solution was fitted to the expression $\delta\alpha(T) = 0.8 + \frac{0.025}{\mathrm{K}}(T - 298\ \mathrm{K})$, where K represents kelvin.[9] An additional consideration of temperature-dependent viscosity $\eta(T)$ showed no significant difference from the linear relation.

Iacopini et al. have demonstrated that the temperature dependence of the Soret coefficient of lysozyme proteins is mainly attributed to nonionic interaction rather than the electrostatic forces (i.e., ionic effects).[60] The Soret coefficient difference $\Delta S_T(T) = |S_T(T) - S_T^{\infty}|$ of proteins was measured under different salinity I, temperature T and protein solubility c_{sat} (Figure 5a). The results show that $\Delta S_T(T)$ and c_{sat} are significantly changed by T and fully correlated with each other under different I values, implying that the Soret coefficient of lysozyme proteins is weakly influenced by electrostatic forces but strongly dependent on their solubility, which could originate from hydrophobic interactions with water. Conversely, Eslahian et al. proposed that the Soret effect of PS beads is different from the dominant nonionic interaction of lysozyme proteins[60] by suggesting that the Soret effect can mainly be determined by the specific-ion effect, which is especially relevant to the diffusiophoresis in the salt gradient and the electrolyte Seebeck effect.[4] The Soret coefficient, S_T, of charged PS beads in NaCl solutions is temperature-dependent and mainly determined by the Seebeck coefficient, S, and the reduced Soret coefficient, α (Figure 5b). It is worth noting that the S_T of the charged PS

https://dx.doi.org/10.1021/acs.langmuir.0c03182
Langmuir 2021, 37, 1315−1336

beads immersed in a NaOH solution is temperature-independent. This further validates the claim that the charge effect plays an essential role in the temperature dependence of the S_T with respect to the PS beads.

Moreover, Reichl et al. combined four molecular mechanisms to analyze the Soret effect on DNA and RNA[71]

$$S_T = S_T^{CM} + S_T^{EL} + S_T^{NI} + 1/T \tag{23}$$

where S_T^{CM} is the double-layer capacity model from local electric fields,[96] S_T^{EL} is for the global electric field that is derived on the basis of eq 8, S_T^{NI} is from eq 22, which describes the temperature dependence of nonionic contributions, and the last term is due to the temperature dependence of the diffusion coefficient. On the basis of this model, Sehnem et al. was able to fit the experimentally obtained S_T of magnetic colloids versus temperature with high accuracy, leading to the conclusion that the temperature dependence of S_T was caused by the electrolyte Seebeck effect and the double-layer energy (Figure 5c).[10] However, in the present stage, the underlying mechanism of S_T's temperature dependence is still elusive, requiring more experiments and theories to elaborate it further.

All of our discussions and inferences about the theories of thermoelectric fields have assumed that the temperature gradient is constant and unidirectional in solutions made of monovalent electrolyte ions. This assumption needs to be modified for practical applicability. Mainly, applications involving asymmetric heating sources such as laser-based or point-probe-based heating to exactly determine and evaluate the particle's response to thermal gradients cannot be based on the previously mentioned assumption. Kollipara et al. have proposed a new framework for estimating the thermoelectric fields in colloidal suspensions by including a laser-based Gaussian heating source and a particle-induced temperature gradient distortion in the thermoelectric force analysis.[23] Specifically, for a PS particle in the CTAC solution, the temperature gradient around the particle must differ from the default gradient (in the absence of the particle) due to the difference in thermal conductivities between the solute and solvent (Figure 6a). Accordingly, eq 8 for the thermoelectric field under a constant external thermal gradient should be changed to $E_T = \frac{k_B T \nabla T}{e}\left[\left(\frac{Z_1 S_{T1}}{N_{agg}} + S_{T2}\right)/\left(1 - \frac{Z_1 S_{T1}}{N_{agg}}\right)\right]$, where S_{T_1} and S_{T_2} are the Soret coefficients of the CTA^+ micelle and chloride ion, respectively; N_{agg} is the number of ions forming a CTA^+ micelle aggregate; and Z_1 is the effective charge on the micelle. The net thermoelectric force is contributed by the tangential component of the thermoelectric field: $\mathbf{F}_{thermoelectric} = \int \sigma E_{T,\parallel}\, dA$ (Figure 6b). Simulations were then performed for a real case of optothermoelectric trapping,[43] where a PS bead was placed around a thermal gradient region that was generated by laser heating on a plasmonic substrate, which was not uniform across the particle (Figure 6c). The force calculation showed that the thermoelectric potential well was $\sim 400 k_B T$ deep for a 1 μm PS bead with a laser power of 0.135 mW, and this value was 2 to 3 orders of magnitude higher than that of optical tweezers (Figure 6d).

Würger and co-workers first revealed that the expression of thermoelectric fields and thermocharge should be related to the distance r from the particle center, the Debye length λ, and the particle radius a if the thermal gradient originates from a heated particle.[6] On the basis of eq 5 and $\nabla T = -\delta T a/r^2$ for a nonionic sphere, a radial thermoelectric field is given by[6]

$$E = -S\delta T \frac{a}{r^2}\left(1 - \frac{r+\lambda}{a+\lambda} e^{(a-r)/\lambda}\right) \tag{24}$$

As shown in Figure 6e, for a given a, the electric field differentiates on the length scale of the Debye length but is convergent to $S\nabla T$ when $r \gg \lambda$. The charge density ρ varies with a similar distance trend. It is worth noting that a sphere with charge Q_P introduces an additional electric field $E_P = Q_P e^{-(r-a)/\lambda}/(4\pi\varepsilon\lambda r)$. Accordingly, this heated-particle-induced Seebeck effect can be utilized to separate carbon nanotubes of different sizes by applying an external electric field E_{ext} due to the drift velocity being related to the radius of the nanotubes.

A subsequent work was developed by Majee and Würger to further discuss the electrolyte Seebeck effect with a three-dimensional temperature field induced by a focused laser beam (Figure 6f).[70] A complete expression of the thermoelectric field is given as

$$E = -S\delta T \frac{a}{r^2}\left[\mathrm{erf}\left(\frac{r}{a}\right) - \frac{1}{2} e^{a^2/4\lambda^2} \times \sum_{\pm}\left(\frac{r}{\lambda} \mp 1\right) e^{\pm r/\lambda}\mathrm{erfc}\left(\frac{a}{2\lambda} \pm \frac{r}{a}\right)\right] \tag{25}$$

where a is the radius of the heated spot and r is the distance from the center of the heated spot. Because the Debye length is defined as $\lambda = (\varepsilon k_B T_0/2e^2 n_0)^{1/2}$, when λ/a is approximately less than 0.3, the thermoelectric field can be regarded as being converged to $S\nabla T$. However, for a micrometer-sized hotspot in a very weak electrolyte, λ is of the same order of magnitude of a, which makes the thermoelectric field vary strictly on the basis of eq 25 (Figure 6g). In addition, it is interesting to find that the thermoelectric field can be built in confined but highly charged geometry (e.g., narrow, highly charged channels) even when based on the ion species with identical thermophoretic mobility, implying that the geometry of the container can also influence the formation of thermoelectric fields.[98]

OPTOTHERMOELECTRIC TECHNOLOGIES AND APPLICATIONS

Progress in the fundamental understanding and control of optothermoelectric effects in colloidal solutions has inspired technological developments. By rationally designing the optical fields, thermal fields, and electrolyte solutions through innovations in materials, optics, and colloidal chemistry, a series of optothermoelectric techniques has been developed for applications in a wide range of fields. Herein, we focus on our recent developments of optothermoelectric trapping, manipulation, pulling, and microswimmers along with their applications in nanofabrication and fundamental studies in nanoscience.

OPTOTHERMOELECTRIC TRAPPING AND MANIPULATION

The light-induced thermoelectric effect was proposed to achieve the directional transport of colloidal particles,[2] micelles,[3] DNA,[71] and so forth.[6,60,61] However, the stable trapping of targeted objects could not be achieved due to poor heat management. Furthermore, because the direction of the thermoelectric field was determined by the electrolyte solution, optothermoelectric trapping was often limited to either positively or negatively charged particles. Recently, Lin et al. developed optothermoelectric tweezers (OTET) in colloidal

https://dx.doi.org/10.1021/acs.langmuir.0c03182
Langmuir 2021, 37, 1315−1336

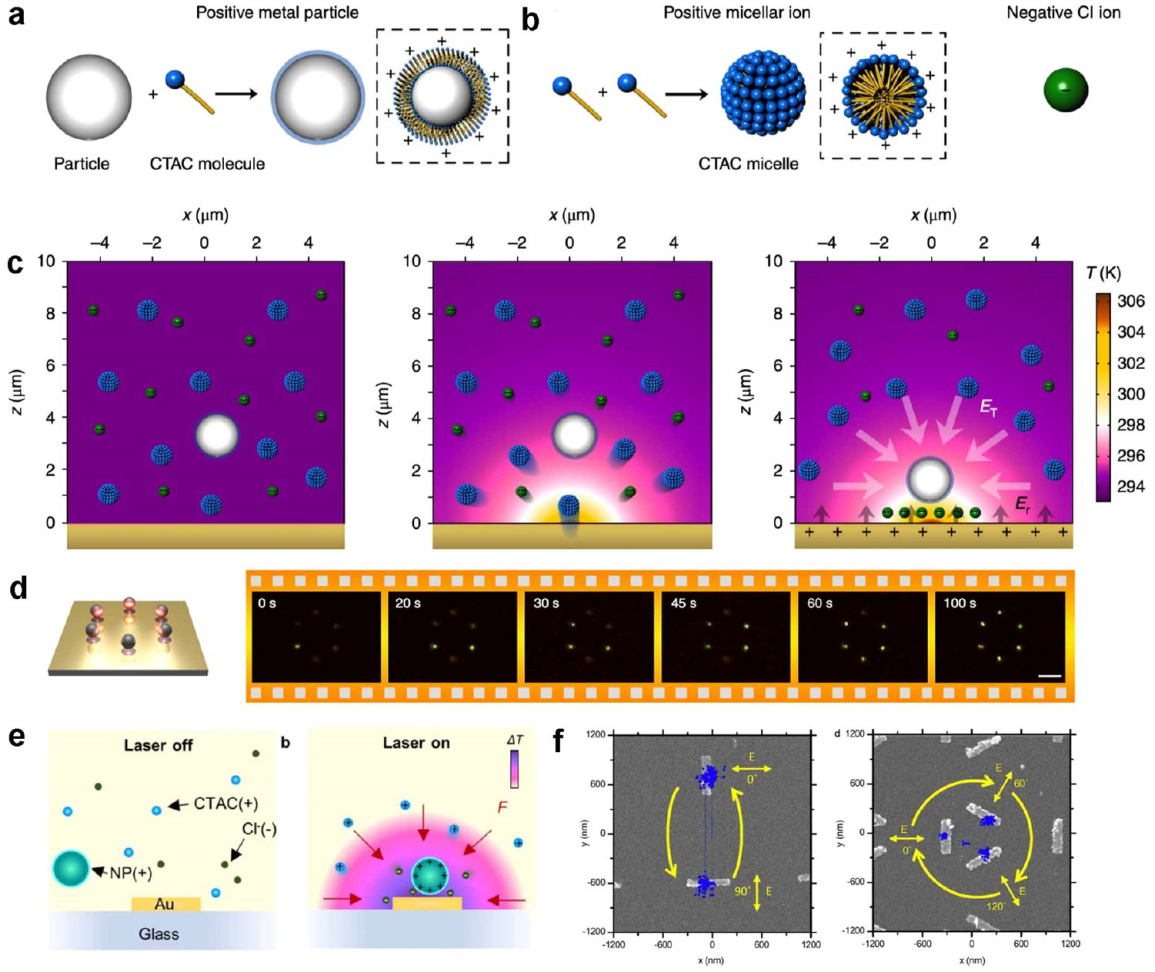

Figure 7. Optothermoelectric trapping and manipulation of colloidal particles. (a) Colloidal particles are adsorbed by CTAC molecules to convert to positively charged surfaces. (b) Positive micellar ions formed by the self-assembly of CTAC molecules (left) and anions offered by Cl^- ions (right). (c) Schematic of optothermoelectric trapping in the sequence: free dispersed particles and ions without optical heating (left), the thermophoretic motion of ions under optical heating (middle), and steady ionic distribution with optical heating to generate a thermoelectric field to trap the positively charged particles (right). (d) Sequential dark-field optical images show the parallel manipulation of six 100 nm silver spheres into a pattern. The scale bar is 5 μm. Adapted with permission from ref 43. Copyright 2018 Springer Nature. (e) Schematic shows optothermoelectric trapping of colloidal nanoparticles on an Au nanorod in a CTAC solution. (f) Linear and circular transportation of 300 nm nanoparticles among different Au nanorods by changing the polarization of the input laser. Adapted with permission from ref 40. Copyright 2018 American Chemical Society.

solutions with added CTAC to trap and manipulate colloidal particles of various compositions, sizes, and shapes at low optical power and with simple optics, regardless of their original surface charge properties.[43] In OTET, all colloidal particles were adsorbed by CTA^+ ions to attain positively charged surfaces (Figure 7a). Meanwhile, when the concentration of CTAC exceeded its critical micellar concentration (0.13−0.16 mM), the CTA^+ ions self-assembled into micelles, and these micelles acted as positive macroions (Figure 7b). When the colloidal solution was on a thermoplasmonic substrate such as AuNIs on a glass slide, which was then exposed to focused laser irradiation, the AuNIs converted the laser incidence to localized radial heating to trigger the ionic redistribution of CTA^+ micelles and Cl^- ions. As the S_T of the micelle was much higher than the S_T of the Cl^- ion ($\sim 10^{-2}$ K^{-1} and 7.18×10^{-4} K^{-1}, respectively), a thermoelectric field pointing to the hotspot (i.e., the maximal laser intensity spot) was established on the basis of eq 8. The positively charged colloidal particles were attracted and trapped at the hotspot (Figure 7c). Since the thermoplasmonic substrate was quasi-continuous, dynamic manipulation of the trapped particles was achieved through movement of the laser beam. Parallel manipulation of multiple single nanoparticles is shown in Figure 7d, which was enabled by a digital micromirror device (DMD) that generated multiple laser beams with simultaneous control.

To overcome the diffraction limit of light and thus enhance the spatial resolution of optothermoelectric trapping, rationally designed plasmonic nanoantennas (i.e., AuNRs) instead of AuNIs were implemented as optothermal nanoradiators to achieve the low-power and deterministic manipulation of nanoparticles at subwavelength resolutions.[40] When an AuNR is irradiated with a laser beam, a highly localized temperature gradient field is formed around the Au nanorod and the resultant thermoelectric field traps the positively charged nanoparticles in the vicinity of the AuNR (Figure 7e). The nanoradiator-mediated OTET can overcome the diffraction limit of light to trap and manipulate nanoparticles with nanoscale accuracy. Since the optothermoelectric trapping operates at low optical power (0.08−1.2 mW/μm^2), the optical scattering forces and adverse thermal effects (e.g., natural convective flow) can be significantly reduced, facilitating the stable trapping of different nanoparticles beyond the diffraction limit of light.

https://dx.doi.org/10.1021/acs.langmuir.0c03182
Langmuir 2021, 37, 1315−1336

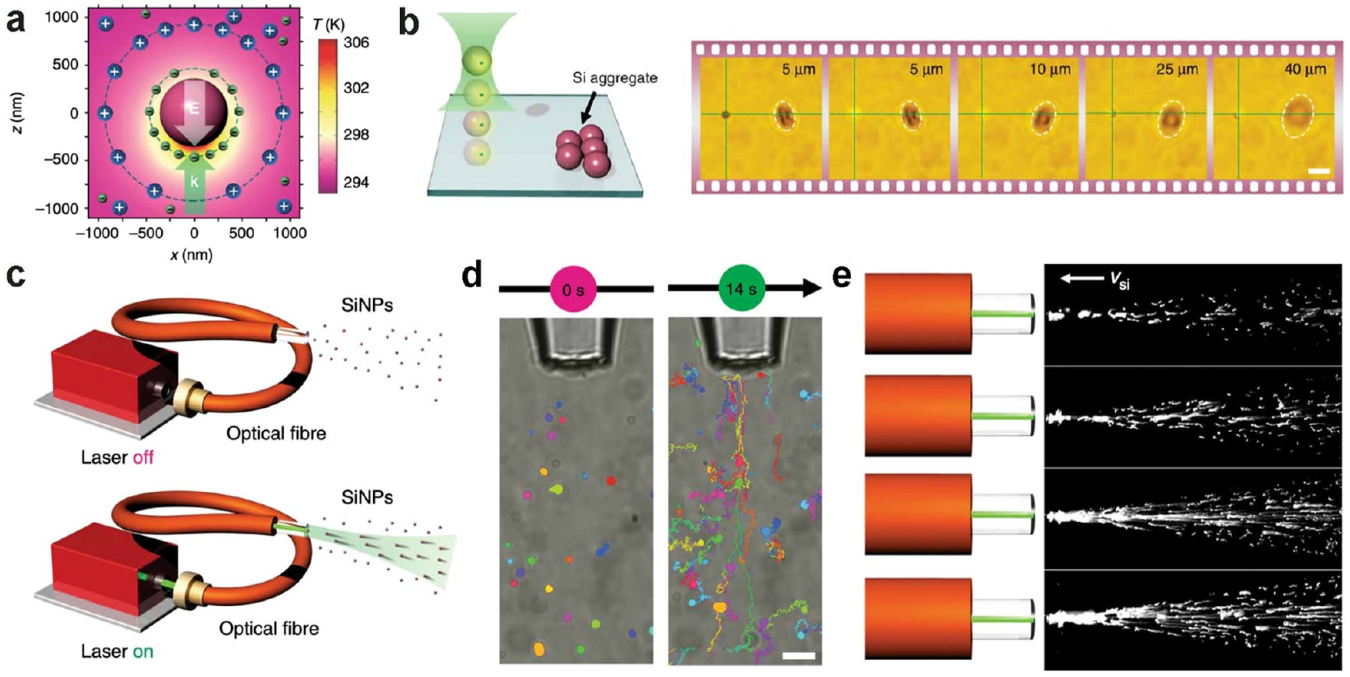

Figure 8. Optothermoelectric pulling and three-dimensional manipulation of colloidal particles. (a) Schematic of the temperature field, spatial ionic distribution, and thermoelectric field generated by a light-absorbing Si particle. (b) Schematic and optical images show the three-dimensional transport of a PS bead via a Si particle that serves as a mobile heating source for OTET. The scale bar is 5 μm. (c) Schematics and (d) optical images of the optothermoelectric pulling of Si particles. (e) Pulling trajectories of 800 nm Si particles in a 1 mM CTAC solution at different optical densities. Adapted with permission from ref 45. Copyright 2020 Springer Nature.

Moreover, the light-generated thermoelectric field and thus the trapping stiffness of this nanoantenna-mediated OTET can be simply modulated by adjusting the polarization of the laser beam. This is because the optical absorption and thus the optothermal conversion efficiency of an anisotropic AuNR with its transversal and longitudinal plasmon resonances at different wavelengths depend upon the polarization of the incident laser beam relative to the AuNR orientation. For example, when a laser beam with a wavelength that matches the transverse plasmon resonance wavelength of the AuNR is applied, the resulting trapping stiffness is highest when the laser beam polarization is perpendicular to the nanorod axis and lowest when the polarization is along the nanorod axis. Accordingly, rationally designed AuNR arrays are fabricated to achieve the directed transport of nanoparticles with nanometer resolution among different nanorods by simply changing the laser beam polarization (Figure 7f). In another development, Kotnala et al. exploited multimode fibers to develop optothermoelectric speckle tweezers for large-scale optothermoelectric manipulation.[42,99] In their demonstration, the output of a multimode fiber led to a speckle light pattern on the AuNI substrate, which generated multiple thermoelectric hotspots to trap numerous nanoparticles simultaneously.[42] Moreover, particle filtration was achieved via the synergistic effects of the optothermoelectric force and the Stokes drag force in microfluidic devices.[99] Compared with other optical manipulation techniques such as optical tweezers,[36] plasmonic tweezers,[100] and optoelectronic tweezers,[17] optothermoelectric manipulations show advantages with respect to their simple optical setup and their applicability to a wide range of polymers, metals, semiconductors, and dielectric nanostructures with different sizes and shapes owing to universally applicable light-driven thermophoresis.

OPTOTHERMOELECTRIC PULLING

The thermoplasmonic substrate is an essential feature of traditional OTET because it facilitates efficient photon−phonon conversion and helps to form a highly localized thermoelectric field. However, the temperature gradient stems from the hotspot on the substrate, making OTET a two-dimensional trapping and manipulation platform. One alternative method for three-dimensional OTET is to transfer the optothermal substrate to an optical fiber platform.[42] As a result, the particles are trapped at the fiber tip due to the thermoelectric field. Three-dimensional particle manipulation is achieved by moving the three-dimensional axis stage to control the position of the fiber tip. By eliminating the need for optical components such as mirrors and lenses, the optothermoelectric fiber tweezers could function as nanopipettes for applications in biosensing and in nanoparticle−cell interaction studies.

Recently, Lin et al. have utilized the optothermoelectric field that stemmed from a single light-absorbing particle to achieve optothermoelectric pulling and three-dimensional manipulation of the particle.[45] When a Si particle in a CTAC solution was irradiated with a focused laser beam, the illuminated half of the particle absorbed more light than the other half, which led to an asymmetric temperature field in the vicinity of the particle. The resultant temperature gradient triggered the spatial redistribution of CTA^+ micelles and Cl^- ions, creating an electric field pointing against the direction of beam propagation (Figure 8a). Since the Si particle was positively charged by CTAC adsorption, the optothermoelectric field could "pull" the particle against the laser propagation direction. At a transition point, where the optothermoelectric force was balanced by the optical scattering force, a particle could be stably trapped, thereby unlocking the three-dimensional manipulation capability of light-absorbing particles through simply repositioning the focal

https://dx.doi.org/10.1021/acs.langmuir.0c03182
Langmuir 2021, 37, 1315−1336

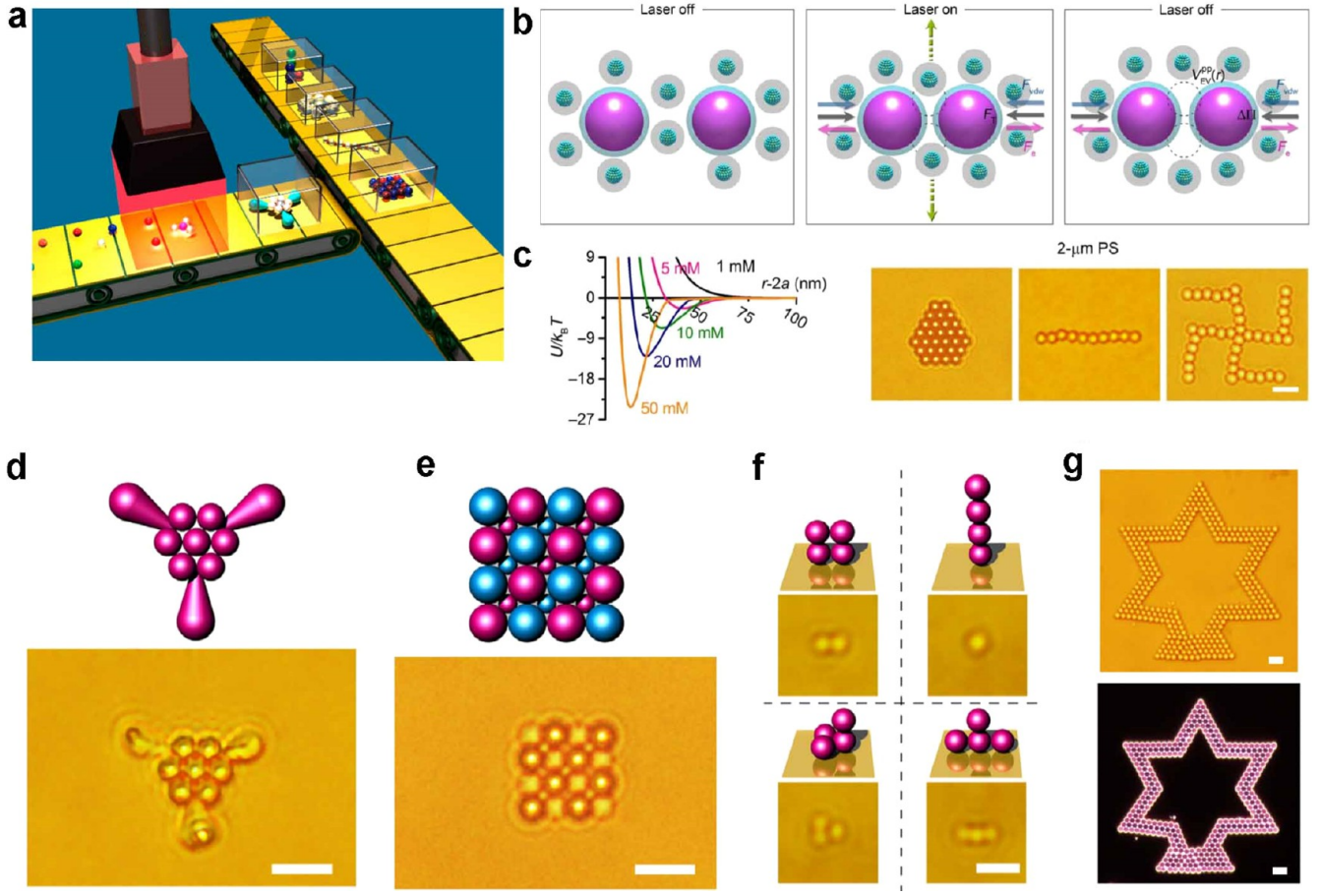

Figure 9. Optothermoelectric assembly of colloidal particles into superstructures. (a) Artistic view of the assembly process with the autonomous delivery of colloidal particles and products. (b) Schematic of the formation of the depletion force between two particles. (c) Interaction potential between two PS beads along with different CTAC concentrations (left) and the optical images of colloidal superstructures. (d) Hybrid assembly of PS beads and anisotropic particles. (e) Hybrid superlattice composed of PS and silica beads of different sizes. (f) Three-dimensional assembly of PS beads. (g) Large-scale assembly of PS beads. The scale bars are 5 μm in (d), (f), and (g) and 2 μm in (f). Adapted with permission from ref 44. Copyright 2017 American Association for the Advancement of Science.

plane of the laser beam. Additionally, the light-absorbing particle could also serve as a mobile heating source for OTET to trap other particles and transport them in three dimensions (Figure 8b). Moreover, when the light source was changed to a laser-coupled tapered optical fiber with a low numerical aperture (NA = 0.1), unconventional long-range trapping (i.e., optothermoelectric pulling) was achieved, which could pull the Si particles toward the laser source over a macroscopic distance (~1 mm) (Figure 8c–e). The self-generated optothermoelectric field on light-absorbing particles provides a new method for the three-dimensional and long-range optothermoelectric manipulation of colloidal particles. Optothermoelectric pulling adds to the field of photophoretic pulling,[101−104] which requires simpler optics.

OPTOTHERMOELECTRIC NANOFABRICATION

Optothermoelectric manipulation can be used to fabricate arbitrary superstructures from colloidal particles as the building blocks where depletion attraction is exploited as the primary binding mechanism to create these structures (Figure 9a).[41,44,105,106] Particle−molecule mixtures can exhibit depletion interactions under a temperature gradient.[107] In a solution, both the electrolytic molecules and the colloidal particles have directional thermophoretic motions under a temperature field. Due to the difference in migration rates, a concentration gradient is created once equilibrium is achieved. Consequently, repulsion from the nonuniform distribution of molecules exerts an osmotic pressure on the particles, driving the particles from the cold to the hot region. Vesicles, micelles, and nanoparticles can also serve as viable depletants to generate depletion forces on the larger colloidal particles.[108] Accordingly, when two particles are trapped at the laser spot by OTET, the temperature gradients induced by laser heating will drive the CTAC micelles out of the interparticle area (Figure 9b). The depletion of the micelles in the gap between particles leads to a depletion attraction that can stably bond the two colloidal particles. The strength of the bonding has been theoretically calculated, and it illustrates a strong dependence on the CTAC concentration (Figure 9c). Furthermore, the bonding between the particles can still exist after the laser is turned off under the condition that the balance among the van der Waals interaction, depletion potential, and electrostatic repulsion produces an attractive potential exceeding several k_BT (Figure 9c).

As shown in Figure 9d,e, various superstructures can be assembled using colloidal particles of a wide range of materials, sizes, and shapes. In addition, optothermal assembly can also achieve complex three-dimensional (Figure 9f) and large-scale two-dimensional superstructures (Figure 9g). Its versatile, low-power, and reliable assembly of colloidal particles makes

https://dx.doi.org/10.1021/acs.langmuir.0c03182
Langmuir 2021, 37, 1315−1336

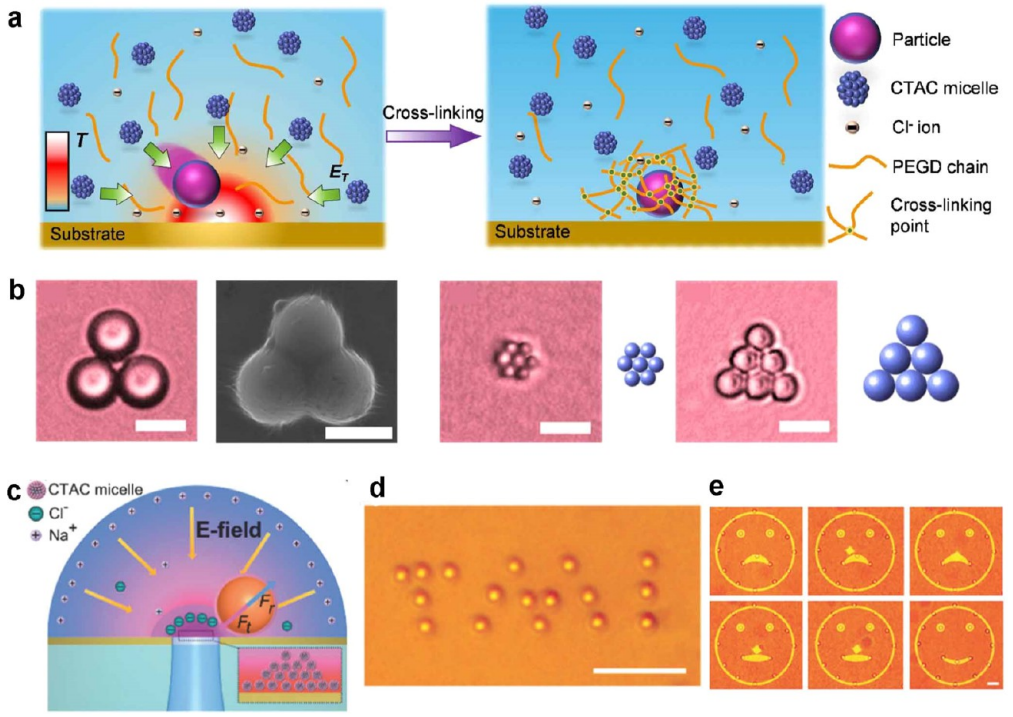

Figure 10. (a) Schematic of optothermoelectric trapping of a colloidal particle followed by its immobilization on the substrate in a photocurable hydrogel solution. (b) Optical images and scanning electron micrographs of immobilized colloidal superstructures. The scale bar is 5 μm. Adapted with permission from ref 106. Copyright 2018 American Chemical Society. (c) Schematic of the optothermoelectric trapping and printing. (d) Optical image of a printed TMI pattern of 1 μm PS spheres on the substrate. The scale bar is 10 μm. (e) Optical images of the reconfigurable printing from a sad face to smiley face. The scale bar is 5 μm. Adapted with permission from ref 41. Copyright 2017 The Royal Society of Chemistry.

Table 2. Brief Comparison of Assembly Techniques for Colloidal Superstructures

techniques	advantages	limitations
optothermal assembly	- no strict restrictions on sizes, materials, or shapes of particles	- small-scale and low-throughput assembly
	- high spatial precision of assembly beyond the diffraction limit of light	- requirement of the heating source
	- low operating power	- tunable interparticle distances in the superstructures
	- simple optical setup	
optical assembly	- high spatial precision of assembly with near-field optics	- small-scale and low-thoroughput assembly
	- versatile three-dimensional assembly	- requirement of rigorous optical setup
	- applicability to various environments (i.e., vacuum, gas, and liquid)	
optoelectronic assembly	- large-scale assembly	- two-dimentional assembly
	- simple optical setup	- requirement of electrolytes
	- low operating power	- requirement of electrical components
electric assembly	- large-scale and high-throughput assembly	- requirement of particles and solvents with specific electric properties
	- simple experimental setup	- Fair spatial precision of assembly
magnetic assembly	- large-scale and high-throughput assembly	- requirement of particles with a magnetic response
		- fair spatial precision of assembly
		- limited types of structures
acoustic assembly	- no strict restrictions on materials and shapes of particles	- difficulty in assembling small collodial particles
	- large-scale and high-throughput assembly	- fair spatial precision of assembly
	- simple experimental setup	
chemical assembly	- high-throughput assembly	- requirement of chemical modifications for particles or substrates
	- stable superstructures	
self-assembly	- large-scale and high-throughput assembly	- limited types of colloidal superstructures
	- simple and cost-effective approach	

optothermoelectric tweezers a promising technology for the rapid prototyping of colloidal materials and devices.

Moreover, the optothermoelectrically assembled colloidal nanostructures can be immobilized on the solid-state substrates for device applications by introducing the photocurable hydrogel into the colloidal solutions.[106] After the assembly process, ultraviolet (UV) light is used to initiate the cross-linking reaction of the hydrogel. The cured hydrogel entraps and immobilizes the particles on the substrate (Figure 10a). The hydrogel-based immobilizing method can be used to form

https://dx.doi.org/10.1021/acs.langmuir.0c03182
Langmuir 2021, 37, 1315−1336

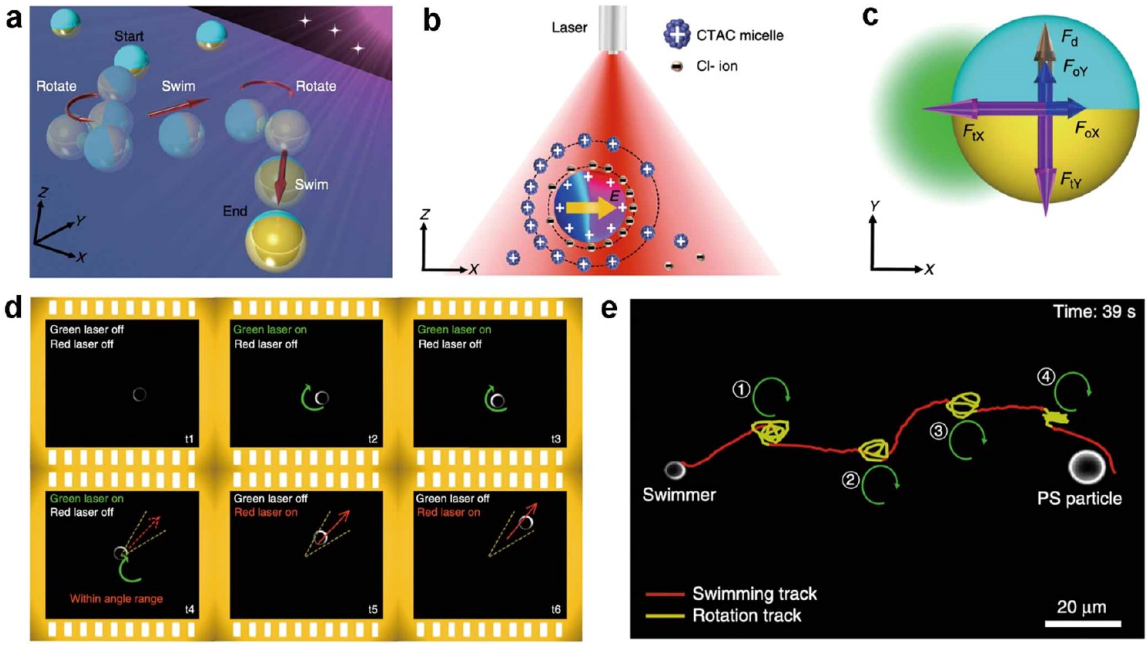

Figure 11. Optothermoelectric microswimmers. (a) Schematic shows that a Janus particle swims and rotates alternatively along a predesigned path via an optothermoelectric field. (b) Steady state of ionic distribution around a Janus particle under an expanded laser beam in a CTAC solution. The resultant thermoelectric field drives the Janus particle to swim along the direction from the Au cap to the unmodified part. (c) Force analysis of a 2.7 μm PS/Au Janus particle rotating around a focused green laser beam. $\mathbf{F}_v$, $\mathbf{F}_o$, and $\mathbf{F}_d$ are thermoelectric force, optical force, and Stokes drag force, respectively. X and Y subscripts indicate the x and y axes. (d) Time-evolved dark-field optical images show one round of rotation and directional swimming behaviors of a Janus particle based on feedback control. (e) Targeted delivery of a 5 μm PS/Au Janus particle to a 10 μm PS particle based on feedback control. Rotation was triggered by a 532 nm laser beam, and swimming was achieved by a 660 nm laser beam. Adapted with permission from ref 46. Copyright 2020 Springer Nature.

various highly stable colloidal patterns on the substrate (Figure 10b).

An alternative approach to immobilizing colloidal particles on substrates is known as optothermoelectric printing, which is based on the depletion attraction between the particle and the substrate.[41] Once a particle is trapped in an optothermoelectric field, an increase in laser power will reduce the particle−substrate gap, causing an increase in the depletion attraction force between them to eventually push the particle toward the substrate (Figure 10c). The osmotic pressure imbalance due to the depletion of CTAC micelles generates a pinning force that bonds the particle to the substrate because of increased van der Waals interactions. When the laser is turned off, the interactions remain strong enough to overcome the repulsive electrostatic force, resulting in stable bonding between the particle and the substrate. Arbitrary superstructures of colloidal particles can be printed on the substrate by this method (Figure 10d). Furthermore, by irradiating the printed particle with an even higher-powered laser beam to allow the CTAC micelles to undergo thermophoresis and reaccumulate at the particle−substrate interface, the depletion binding force is weakened and the particle can be released from its initial printed position. As illustrated in Figure 10e, one of the printed particles was released and then reprinted at a new target location, achieving reconfigurable printing. A brief comparison among different assembly techniques for colloidal superstructures, which includes both optical methods[109−112] and other commonly applied methods, is shown in Table 2.

OPTOTHERMOELECTRIC MICROSWIMMERS

Taking advantage of their asymmetric optothermal response, Janus particles have already been exploited as micro/nano-swimmers based on self-thermophoresis,[55,57,113] diffusiophoresis,[30,54] and electrophoresis,[114] which have inspired various applications in cargo delivery, micro/nanorobots, environment remediation, and so forth.[115−118] Recently, Peng et al. have exploited the thermoelectric effect and feedback control method to develop a new version of dual-state microswimmers based on Janus particles (Figure 11a).[46] The Janus particles were PS microspheres with half-coated metallic caps (i.e., Au) and were dispersed in the CTAC solutions. When an expanded laser beam irradiated the Janus particle, a temperature gradient was created around the surface of the particle due to the different light absorptivity between PS and Au halves. The temperature gradient caused the ionic redistribution to obtain a thermoelectric field pointing from the metallic cap to its counterpart (PS half) for directional swimming of the Janus particle (Figure 11b). Once the swimming direction was disturbed by rotational Brownian motion, the expanded laser beam was switched to a focused laser beam of a different wavelength to induce the in-plane rotation of the Janus particle through the synergistic effect of thermoelectric, optical, and Stokes drag forces (Figure 11c). The timing of the switch between the swimming and rotational states was subtly controlled by a home-built feedback control algorithm, by which the lost Janus particle could recover to the predesigned path by a systematic swimming−rotation−swimming loop (Figure 11d). As an example, a 5 μm Au/PS Janus particle was delivered to a predesigned target over 110 μm in 39 s (Figure 11e). Featuring two working states that can be easily switched via the different laser inputs, the optothermoelectric swimmers are complementary to other light-driven microswimmers.[119,120]

https://dx.doi.org/10.1021/acs.langmuir.0c03182
Langmuir 2021, 37, 1315−1336

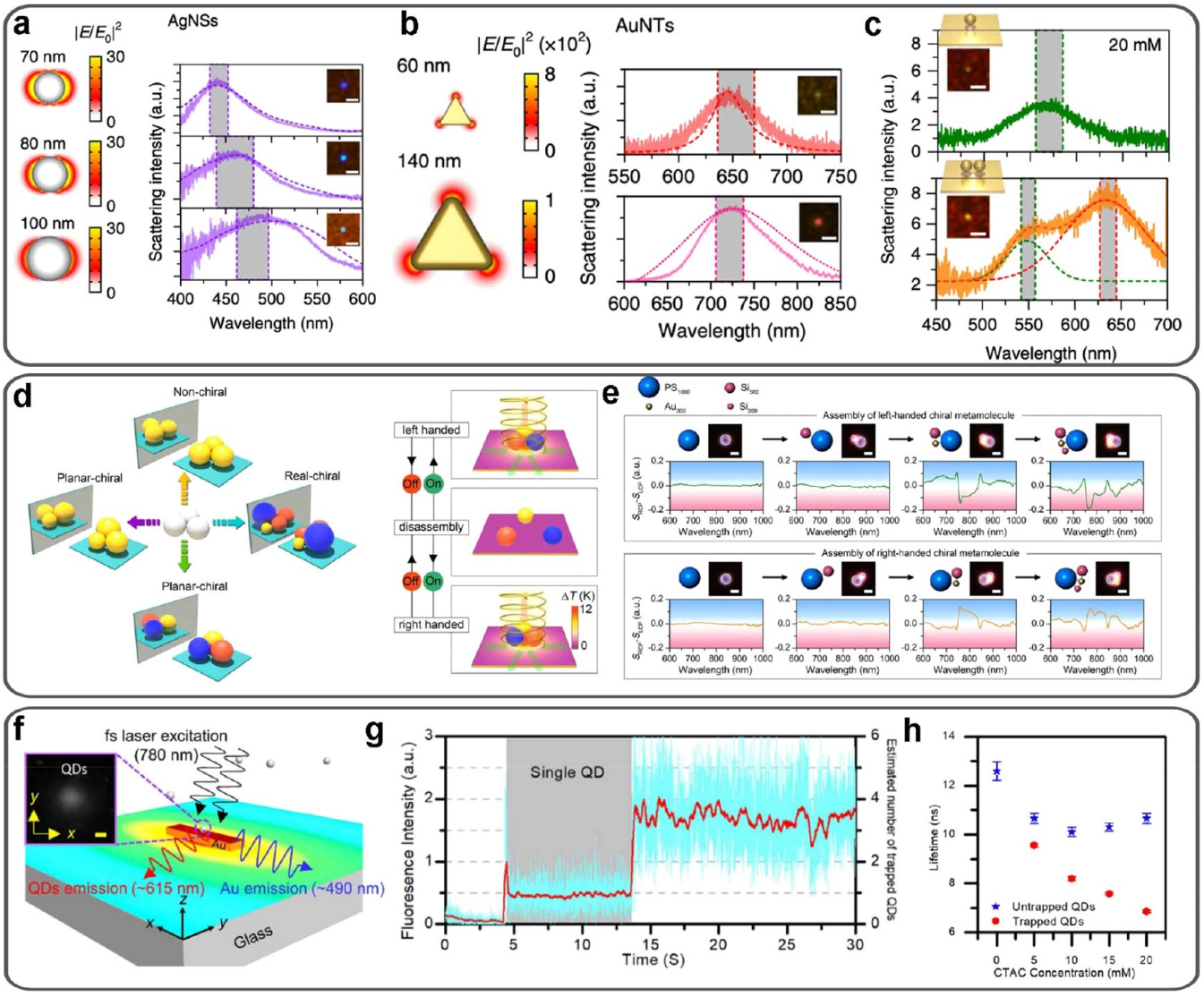

Figure 12. Fundamental studies in nanophotonics enabled by optothermoelectric tweezers. Dark-field optical images, experimental and simulated scattering spectra, and electric field profiles of (a) single Ag nanospheres with diameters of 70, 80, and 100 nm and (b) single Au nanotriangles with side lengths of 60 and 140 nm. (c) Dark-field optical images and scattering spectra of a single Au nanosphere (top) and two coupled Au nanospheres (bottom). Adapted with permission from ref 43. Copyright 2018 Springer Nature. (d) Schematic of the working principle of the reconfigurable chiral meta-molecules based on OTET. (e) Schematics, optical images, and differential scattering spectra of each configuration during the assembly of chiral meta-molecules. Adapted with permission from ref 123. Copyright 2019 Elsevier. (f) Schematic of the emission lifetime measurement for the quantum dots optothermoelectrically trapped at the Au nanorod. (g) Fluorescence intensity and estimated number of quantum dots trapped on a single Au nanorod as a function of time. (h) Fluorescence lifetimes of free and trapped quantum dots at different CTAC concentrations. Adapted with permission from ref 40. Copyright 2018 American Chemical Society.

OPTOTHERMOELECTRIC TECHNOLOGIES IN NANOSCIENCE

With their versatile capabilities of manipulating nanoparticles of various compositions, sizes, and shapes at low optical power and with simple optics, optothermoelectric technologies are well suited for investigating the fundamental phenomena at the nanoscale. Herein, we highlight our recent work on studying light−matter interactions at the nanoscale with optothermoelectric tweezers.

In Situ Optical Spectroscopy for Colloidal Nanoparticles in Solutions. Optical scattering spectra of metal nanoparticles can be used to study their size, composition, morphology, and plasmonic coupling. However, it is challenging to directly record the scattering spectra of metal nanoparticles in solution due to their strong Brownian motion. Traditional optical trapping of metal nanoparticles has critical requirements for the laser wavelength, which may interfere with the optical scattering measurement of the trapped nanoparticles. In contrast, metal nanoparticles can be stably trapped via OTET with variable working wavelengths for in situ optical scattering measurements.[43] As shown in Figure 12a,b, OTET has been successfully applied to trapping metal nanoparticles of varying geometric shapes and sizes for the in situ recording of their scattering spectra in solutions. The operational laser wavelength of OTET was chosen to avoid the overlap with the scattering peaks of the nanoparticles. This in situ optical spectroscopy can also be used to detect the optical coupling between metal nanoparticles (Figure 12c).

Chirality of Colloidal Metamolecules. Chirality represents the property of an object that is nonsuperimposable on its

https://dx.doi.org/10.1021/acs.langmuir.0c03182
Langmuir 2021, 37, 1315−1336

mirror image, which shows handedness-dependent responses under the irradiation of circularly polarized light.[121,122] By mimicking chiral molecules in chemistry, optical chiral meta-molecules can be assembled via OTET using colloidal particles as the meta-atoms.[123] As shown in Figure 12d, colloidal particles can be assembled into chiral meta-molecules with different geometries and reassembled into their enantiomers due to reversible micelle-mediated colloidal bonding. The differential scattering spectra under circularly polarized irradiation shown in Figure 12e indicate that both geometric and compositional asymmetries can alter the optical chirality of meta-molecules. It should be noted that the optical chirality can be partially changed by alternating the location of certain colloidal components in the meta-molecules, which can promote a more comprehensive understanding of the origin of optical chirality on the colloidal scale.

Lifetime Measurement for Single Quantum Dots at Plasmonic Nanoantennas. OTET based on Au nanoantennas has been exploited for the in situ characterization of different quantum dots (QDs) at low operational power.[40] With the help of femtosecond laser heating to provide a much stronger temperature gradient, optothermoelectric trapping of QDs on AuNRs has been achieved far beyond the diffraction limit of light (Figure 12f). By recording the two-photon fluorescence signal from the trapped QDs, the number of trapped QDs can be quantitatively estimated (Figure 12g). Furthermore, the lifetime of trapped and untrapped QDs was plotted and compared at various CTAC concentrations. Figure 12h shows that the lifetime of nontrapped QDs decreases with CTAC concentration until reaching a constant mean lifetime of 10.5 ns while the mean lifetime of the trapped QDs continually decreased as the CTAC concentration increased, which can be attributed to the reduction of the QD−nanorod distance and the resultant enhancement of the plasmon−exciton interaction.

CONCLUSIONS

Numerous works have been carried out to elucidate the fundamental mechanisms of the formation of thermoelectric fields in electrolyte solutions and their influence on the migration of colloidal particles under unidirectional constant temperature gradients. Recent research has provided further theories on the interplay between thermoelectricity and colloidal particles in terms of electrolyte properties, particle properties, and temperature field profiles, which underpin newly developed optothermoelectric technologies and their applications. Through tailoring the electrolyte composition, heating substrate, light source, and particle property, the optothermoelectric field has been exploited for versatile particle manipulation with the advantages of low operational power, simple optics, and applicability to various types of particles. Such optothermoelectric manipulations have been proven to be effective in the directed assembly of colloidal particles into superstructures and fundamental studies in nanoscience. The manipulation techniques are also on track to accelerate progress in colloidal sciences and life sciences as well as lab-on-a-chip devices synergizing fluidics, optics, thermal science, and electronics at the micro/nanoscale. With the advancements in fundamentals, technologies, and applications, liquid optothermoelectrics is emerging as an exciting field. We conclude this Invited Feature Article with our perspectives on the challenges and opportunities in the field of liquid optothermoelectrics.

To better understand thermoelectricity in the more complex colloidal systems, one should improve current models that were based on monovalent electrolytes under a constant unidirectional temperature gradient. For example, simply increasing the complexity of electrolyte solutions could result in unknown nonlinear effects between thermophoresis and the resultant thermo-osmosis and thermo-electrophoresis. Such nontrivial effects would make most of the existing models for electrolyte thermoelectricity invalid. Moreover, current thermoelectric theories for colloidal solutions assume that particles have impenetrable surfaces and that no ions can diffuse across the particle surfaces. However, this assumption is no longer valid for colloidal solutions such as those with interacting biological cells and nanoparticles as drug delivery systems. It was observed that the relationship between the surface charge and zeta potential for biological cells could deviate from Gouy−Chapmann theory because of the porous cell membranes allowing ions to diffuse across the cells.[124] Thus, new theories that can take into account the effects of penetrable surfaces of particles under thermoelectric fields will be needed to guide the applications of optothermoelectric technologies in nanobiomedicine and cellular biology.

Much has remained unknown in the optothermoelectric manipulations of colloidal particles. For instance, when using micellar solutions to optothermoelectrically trap a particle based on an immobilized light-absorbing substrate, the adsorbed surfactant molecules on the particle and substrate may result in an unconventional change in the electrical permittivity of the solvent between the particle and substrate,[125] which stems from an undefined relationship between the polarizability of the solvent and the thermoelectric field due to the surfactant molecules in close proximity. The polarizability of the colloidal particles could also significantly affect the optothermoelectric manipulations, which has not been explored in full. In a study on electrophoresis, the induced polarizability of a colloidal particle was shown to depend on the magnitude of the electric current, making it possible to change the particle's migration direction by controlling the current magnitude rather than the current direction.[126] Therefore, a better understanding of field-dependent polarizability of particles could lead to a new dimension of control for optothermoelectric manipulations, which will be based on the incident laser power that determines the amplitude of the optically generated thermoelectric field.

More research is needed to clarify the effects of interactions among various solutes on the optothermoelectricity. It was observed that macroions such as micelles experienced motion that was independent of the motion of counterions under a temperature gradient.[12] In contrast, DNA-coated PS beads might respond differently to the temperature gradient in the presence of surfactants because the surfactants could change the solvent−bead interaction and the zeta potential of the beads and could cause DNA compaction on the PS beads.[127] The DNA compaction can also change the particle−solvent and particle−substrate interactions. Therefore, it becomes necessary to identify all relevant parameters among diverse particles, macroions, counterions, and substrates and explore their interrelationships that are relevant to thermoelectricity.

Improving the optothermoelectric technologies for a broader range of applications will also require new innovations in chemistry, materials, and optics. So far, CTAC has been widely used in optothermoelectric manipulations because it can assist the formation of thermoelectric fields and modify the surfaces of suspended particles to be positively charged. However, CTAC is lethal to most biological cells, which hinders the biological applications of the optothermoelectric manipulations. Recently,

https://dx.doi.org/10.1021/acs.langmuir.0c03182
Langmuir 2021, 37, 1315−1336

Ding et al. have proved that poly(diallyldimethylammonium chloride) (PDADMAC) can replace CTAC in the OTET to enhance both the particle-trapping capability and biocompatibility.[24] To further broaden the applicability of the optothermoelectric manipulations, one may look more into biocompatible electrolytes with ions having considerably different Soret coefficients that can modify the surface charge of the particles.

As demonstrated by Janus particles as microswimmers[46] and plasmonic nanoantennas (i.e., AuNRs) as optothermal nanoradiators,[40] the rational design of the light-absorbing substrates and particles is effective at enhancing the accuracy and versatility of the optothermoelectric manipulations. It has been proven that photonic crystals[128] and metasurfaces[18] can enhance photothermal effects for particle manipulation with a lower operational power and a higher manipulation accuracy. We expect more works on optothermoelectrics that employ designed nanostructures such as photonic crystals, metasurfaces, and metamaterials[129,130] in immobilized light-absorbing substrates with enhanced optical generation and the control of temperature fields.[21] Benefiting from advancements in colloidal chemistry, one anticipates the exploration of a variety of suspended light-absorbing particles[131] to further the fundamental understanding and applications of optothermoelectrics. These particles can be modified with functional groups to enhance their applications in drug delivery and biosensing.[132−134]

AUTHOR INFORMATION

Corresponding Author

Yuebing Zheng − *Materials Science & Engineering Program and Texas Materials Institute and Walker Department of Mechanical Engineering, The University of Texas at Austin, Austin, Texas 78712, United States;* orcid.org/0000-0002-9168-9477; Email: zheng@austin.utexas.edu

Authors

Zhihan Chen − *Materials Science & Engineering Program and Texas Materials Institute, The University of Texas at Austin, Austin, Texas 78712, United States*

Pavana Siddhartha Kollipara − *Walker Department of Mechanical Engineering, The University of Texas at Austin, Austin, Texas 78712, United States;* orcid.org/0000-0003-0166-6720

Hongru Ding − *Walker Department of Mechanical Engineering, The University of Texas at Austin, Austin, Texas 78712, United States;* orcid.org/0000-0003-1579-6825

Agatian Pughazhendi − *Walker Department of Mechanical Engineering, The University of Texas at Austin, Austin, Texas 78712, United States*

Complete contact information is available at: https://pubs.acs.org/10.1021/acs.langmuir.0c03182

Author Contributions

All authors listed have made a substantial, direct, and intellectual contribution to the work and approved it for publication.

Notes

The authors declare no competing financial interest.

Biographies

Zhihan Chen is a Ph.D. student at the Texas Materials Institute in The University of Texas at Austin, working in Dr. Yuebing Zheng's group. He received his B.S. in materials science and engineering at Shanghai Jiao Tong University in 2018. His research interests lie in optical microswimmers and the intelligent manipulation of micro/nanoparticles.

Pavana Siddhartha Kollipara is a graduate student, pursuing his doctoral studies under the supervision of Dr. Yuebing Zheng in the Walker Department of Mechanical Engineering at the University of Texas at Austin. He received his B.Tech and M.Tech degrees in mechanical engineering at the Indian Insitute of Technology, Madras, in 2017. His current research interests are thermoelectricity, optical trapping and manipulation of colloids, optical lithography, and light−matter interactions.

Hongru Ding is currently a Ph.D. student in the Walker Department of Mechanical Engineering at The University of Texas at Austin. He obtained his B.S. degree in energy and power engineering in 2015 and

https://dx.doi.org/10.1021/acs.langmuir.0c03182
Langmuir 2021, 37, 1315−1336

his M.S. degree in engineering thermophysics in 2018, both from Huazhong University of Science and Technology, Wuhan, China. Supported by an Australian Endeavour Leadership Program research fellowship, he visited The University of Sydney, Australia for half a year. His current research interest focuses on the optothermal manipulation of micro/nanoparticles.

Agatian Pughazhendi is pursuing his bachelor's degree in mechanical engineering and computer science from The University of Texas at Austin. Currently, his research focuses on optothermoelectric methods to achieve nanoresolution particle manipulation and assembly. His scientific interests include materials and design engineering, the development of space technology, and sustainability.

Yuebing Zheng is an associate professor of mechanical engineering and materials science & engineering at the University of Texas at Austin. He also holds the William W. Hagerty Endowed Faculty Fellowship in Engineering. He received his Ph.D. in engineering science and mechanics from The Pennsylvania State University in 2010. He was a postdoctoral researcher at the University of California, Los Angeles, from 2010 to 2013. His research group explores intelligent nano-optofluidics, which merges photonics, fluidics, and artificial intelligence at the nanoscale, to innovate research tools and address grand challenges for engineering.

■ ACKNOWLEDGMENTS

The authors acknowledge the financial support of the National Science Foundation (NSF-CMMI-1761743 and NSF-ECCS-2001650), the National Aeronautics and Space Administration (80NSSC17K0520), and the National Institute of General Medical Sciences of the National Institutes of Health (DP2GM128446).

■ REFERENCES

(1) Putnam, S. A.; Cahill, D. G. Transport of Nanoscale Latex Spheres in a Temperature Gradient. *Langmuir* **2005**, *21* (12), 5317−5323.
(2) Würger, A. Transport in Charged Colloids Driven by Thermoelectricity. *Phys. Rev. Lett.* **2008**, *101* (10), 108302.
(3) Vigolo, D.; Buzzaccaro, S.; Piazza, R. Thermophoresis and Thermoelectricity in Surfactant Solutions. *Langmuir* **2010**, *26* (11), 7792−7801.
(4) Eslahian, K. A.; Majee, A.; Maskos, M.; Würger, A. Specific Salt Effects on Thermophoresis of Charged Colloids. *Soft Matter* **2014**, *10* (12), 1931−1936.
(5) Würger, A. Thermal Non-Equilibrium Transport in Colloids. *Rep. Prog. Phys.* **2010**, *73* (12), 126601.
(6) Majee, A.; Würger, A. Charging of Heated Colloidal Particles Using the Electrolyte Seebeck Effect. *Phys. Rev. Lett.* **2012**, *108* (11), 118301.
(7) Chikina, I.; Shikin, V.; Varlamov, A. A. Seebeck Effect in Electrolytes. *Phys. Rev. E* **2012**, *86* (1), 011505.
(8) Piazza, R.; Guarino, A. Soret Effect in Interacting Micellar Solutions. *Phys. Rev. Lett.* **2002**, *88* (20), 208302.
(9) Würger, A. Temperature Dependence of the Soret Motion in Colloids. *Langmuir* **2009**, *25* (12), 6696−6701.
(10) Sehnem, A.; Neto, A. F.; Aquino, R.; Campos, A.; Tourinho, F.; Depeyrot, J. Temperature Dependence of the Soret Coefficient of Ionic Colloids. *Phys. Rev. E* **2015**, *92* (4), 042311.
(11) Braibanti, M.; Vigolo, D.; Piazza, R. Does Thermophoretic Mobility Depend on Particle Size? *Phys. Rev. Lett.* **2008**, *100* (10), 108303.
(12) Morthomas, J.; Würger, A. Thermoelectric Effect on Charged Colloids in the Hückel Limit. *Eur. Phys. J. E: Soft Matter Biol. Phys.* **2008**, *27* (4), 425−434.
(13) Majee, A.; Würger, A. Collective Thermoelectrophoresis of Charged Colloids. *Phys. Rev. E* **2011**, *83* (6), 061403.
(14) Lüsebrink, D.; Ripoll, M. Collective Thermodiffusion of Colloidal Suspensions. *J. Chem. Phys.* **2012**, *137* (19), 194904.
(15) Ashkin, A.; Dziedzic, J. M.; Bjorkholm, J. E.; Chu, S. Observation of a Single-Beam Gradient Force Optical Trap for Dielectric Particles. *Opt. Lett.* **1986**, *11* (5), 288−290.
(16) Juan, M. L.; Righini, M.; Quidant, R. Plasmon Nano-Optical Tweezers. *Nat. Photonics* **2011**, *5* (6), 349−356.
(17) Wu, M. C. Optoelectronic Tweezers. *Nat. Photonics* **2011**, *5* (6), 322−324.
(18) Hong, C.; Yang, S.; Ndukaife, J. C. Stand-Off Trapping and Manipulation of Sub-10 Nm Objects and Biomolecules Using Opto-Thermo-Electrohydrodynamic Tweezers. *Nat. Nanotechnol.* **2020**, *15* (11), 908−913.
(19) Baffou, G.; Quidant, R.; García de Abajo, F. J. Nanoscale Control of Optical Heating in Complex Plasmonic Systems. *ACS Nano* **2010**, *4* (2), 709−716.
(20) Krasnok, A.; Caldarola, M.; Bonod, N.; Alú, A. Spectroscopy and Biosensing with Optically Resonant Dielectric Nanostructures. *Adv. Opt. Mater.* **2018**, *6* (5), 1701094.
(21) Jauffred, L.; Samadi, A.; Klingberg, H.; Bendix, P. M.; Oddershede, L. B. Plasmonic Heating of Nanostructures. *Chem. Rev.* **2019**, *119* (13), 8087−8130.
(22) Ly, A.; Majee, A.; Würger, A. Nanoscale Seebeck Effect at Hot Metal Nanostructures. *New J. Phys.* **2018**, *20* (2), 025001.
(23) Kollipara, P. S.; Lin, L.; Zheng, Y. Thermo-Electro-Mechanics at Individual Particles in Complex Colloidal Systems. *J. Phys. Chem. C* **2019**, *123* (35), 21639−21644.
(24) Ding, H.; Kollipara, P. S.; Lin, L.; Zheng, Y. Atomistic Modeling and Rational Design of Optothermal Tweezers for Targeted Applications. *Nano Res.* **2021**, *14*, 295−303.
(25) Li, J.; Lin, L.; Inoue, Y.; Zheng, Y. Opto-Thermophoretic Tweezers and Assembly. *J. Micro Nano-Manufacturing* **2018**, *6* (4), DOI: 10.1115/1.4041615.
(26) Lin, L.; Hill, E. H.; Peng, X.; Zheng, Y. Optothermal Manipulations of Colloidal Particles and Living Cells. *Acc. Chem. Res.* **2018**, *51* (6), 1465−1474.

https://dx.doi.org/10.1021/acs.langmuir.0c03182
Langmuir 2021, 37, 1315−1336

(27) Pughazhendi, A.; Chen, Z.; Wu, Z.; Li, J.; Zheng, Y. Opto-Thermoelectric Tweezers: Principles and Applications. *Front. Phys.* **2020**, *8* (468), DOI: 10.3389/fphy.2020.580014.
(28) Buttinoni, I.; Volpe, G.; Kümmel, F.; Volpe, G.; Bechinger, C. Active Brownian Motion Tunable by Light. *J. Phys.: Condens. Matter* **2012**, *24* (28), 284129.
(29) Volpe, G.; Buttinoni, I.; Vogt, D.; Kümmerer, H.-J.; Bechinger, C. Microswimmers in Patterned Environments. *Soft Matter* **2011**, *7* (19), 8810−8815.
(30) Lozano, C.; Ten Hagen, B.; Löwen, H.; Bechinger, C. Phototaxis of Synthetic Microswimmers in Optical Landscapes. *Nat. Commun.* **2016**, *7* (1), 12828.
(31) Zhang, J.; Yan, J.; Granick, S. Directed Self-Assembly Pathways of Active Colloidal Clusters. *Angew. Chem.* **2016**, *128* (17), 5252−5255.
(32) Yan, J.; Han, M.; Zhang, J.; Xu, C.; Luijten, E.; Granick, S. Reconfiguring Active Particles by Electrostatic Imbalance. *Nat. Mater.* **2016**, *15* (10), 1095−1099.
(33) Voldman, J. Electrical Forces for Microscale Cell Manipulation. *Annu. Rev. Biomed. Eng.* **2006**, *8*, 425−454.
(34) Ozcelik, A.; Rufo, J.; Guo, F.; Gu, Y.; Li, P.; Lata, J.; Huang, T. J. Acoustic Tweezers for the Life Sciences. *Nat. Methods* **2018**, *15* (12), 1021−1028.
(35) Tian, Z.; Yang, S.; Huang, P.-H.; Wang, Z.; Zhang, P.; Gu, Y.; Bachman, H.; Chen, C.; Wu, M.; Xie, Y.; Huang, T. J. Wave Number-Spiral Acoustic Tweezers for Dynamic and Reconfigurable Manipulation of Particles and Cells. *Science Advances* **2019**, *5* (5), No. eaau6062.
(36) Ashkin, A.; Dziedzic, J. M.; Yamane, T. Optical Trapping and Manipulation of Single Cells Using Infrared Laser Beams. *Nature* **1987**, *330* (6150), 769−771.
(37) Ashkin, A.; Dziedzic, J. M. Optical Trapping and Manipulation of Viruses and Bacteria. *Science* **1987**, *235* (4795), 1517.
(38) Fan, X.; White, I. M. Optofluidic Microsystems for Chemical and Biological Analysis. *Nat. Photonics* **2011**, *5* (10), 591−597.
(39) Chen, J.; Loo, J. F.-C.; Wang, D.; Zhang, Y.; Kong, S.-K.; Ho, H.-P. Thermal Optofluidics: Principles and Applications. *Adv. Opt. Mater.* **2020**, *8* (1), 1900829.
(40) Liu, Y.; Lin, L.; Bangalore Rajeeva, B.; Jarrett, J. W.; Li, X.; Peng, X.; Kollipara, P.; Yao, K.; Akinwande, D.; Dunn, A. K. Nanoradiator-Mediated Deterministic Opto-Thermoelectric Manipulation. *ACS Nano* **2018**, *12* (10), 10383−10392.
(41) Lin, L.; Peng, X.; Zheng, Y. Reconfigurable Opto-Thermoelectric Printing of Colloidal Particles. *Chem. Commun.* **2017**, *53* (53), 7357−7360.
(42) Kotnala, A.; Zheng, Y. Opto-Thermophoretic Fiber Tweezers. *Nanophotonics* **2019**, *8* (3), 475−485.
(43) Lin, L.; Wang, M.; Peng, X.; Lissek, E. N.; Mao, Z.; Scarabelli, L.; Adkins, E.; Coskun, S.; Unalan, H. E.; Korgel, B. A.; Liz-Marzán, L. M.; Florin, E.-L.; Zheng, Y. Opto-Thermoelectric Nanotweezers. *Nat. Photonics* **2018**, *12* (4), 195−201.
(44) Lin, L.; Zhang, J.; Peng, X.; Wu, Z.; Coughlan, A. C.; Mao, Z.; Bevan, M. A.; Zheng, Y. Opto-Thermophoretic Assembly of Colloidal Matter. *Science Advances* **2017**, *3* (9), No. e1700458.
(45) Lin, L.; Kollipara, P. S.; Kotnala, A.; Jiang, T.; Liu, Y.; Peng, X.; Korgel, B. A.; Zheng, Y. Opto-Thermoelectric Pulling of Light-Absorbing Particles. *Light: Sci. Appl.* **2020**, *9* (1), 34.
(46) Peng, X.; Chen, Z.; Kollipara, P. S.; Liu, Y.; Fang, J.; Lin, L.; Zheng, Y. Opto-Thermoelectric Microswimmers. *Light: Sci. Appl.* **2020**, *9* (1), 141.
(47) Quinten, M. *Optical Properties of Nanoparticle Systems: Mie and Beyond*; John Wiley & Sons: 2010.
(48) Baffou, G.; Quidant, R.; Girard, C. Heat Generation in Plasmonic Nanostructures: Influence of Morphology. *Appl. Phys. Lett.* **2009**, *94* (15), 153109.
(49) Bohren, C. F.; Huffman, D. R. *Absorption and Scattering of Light by Small Particles*; John Wiley & Sons: 2008.
(50) Parsons, J.; Burrows, C.; Sambles, J.; Barnes, W. A Comparison of Techniques Used to Simulate the Scattering of Electromagnetic Radiation by Metallic Nanostructures. *J. Mod. Opt.* **2010**, *57* (5), 356−365.
(51) Kang, Z.; Chen, J.; Wu, S.-Y.; Chen, K.; Kong, S.-K.; Yong, K.-T.; Ho, H.-P. Trapping and Assembling of Particles and Live Cells on Large-Scale Random Gold Nano-Island Substrates. *Sci. Rep.* **2015**, *5* (1), 9978.
(52) Sun, H.; Yu, M.; Wang, G.; Sun, X.; Lian, J. Temperature-Dependent Morphology Evolution and Surface Plasmon Absorption of Ultrathin Gold Island Films. *J. Phys. Chem. C* **2012**, *116* (16), 9000−9008.
(53) Ma, H.; Bendix, P. M.; Oddershede, L. B. Large-Scale Orientation Dependent Heating from a Single Irradiated Gold Nanorod. *Nano Lett.* **2012**, *12* (8), 3954−3960.
(54) Bickel, T.; Majee, A.; Würger, A. Flow Pattern in the Vicinity of Self-Propelling Hot Janus Particles. *Phys. Rev. E* **2013**, *88* (1), 012301.
(55) Jiang, H.-R.; Yoshinaga, N.; Sano, M. Active Motion of a Janus Particle by Self-Thermophoresis in a Defocused Laser Beam. *Phys. Rev. Lett.* **2010**, *105* (26), 268302.
(56) Pierce, D. T.; Spicer, W. E. Electronic Structure of Amorphous Si from Photoemission and Optical Studies. *Phys. Rev. B* **1972**, *5* (8), 3017.
(57) Khadka, U.; Holubec, V.; Yang, H.; Cichos, F. Active Particles Bound by Information Flows. *Nat. Commun.* **2018**, *9* (1), 3864.
(58) Lin, L.; Peng, X.; Wei, X.; Mao, Z.; Xie, C.; Zheng, Y. Thermophoretic Tweezers for Low-Power and Versatile Manipulation of Biological Cells. *ACS Nano* **2017**, *11* (3), 3147−3154.
(59) Piazza, R. 'Thermal Forces': Colloids in Temperature Gradients. *J. Phys.: Condens. Matter* **2004**, *16* (38), S4195.
(60) Iacopini, S.; Piazza, R. Thermophoresis in Protein Solutions. *Europhys. Lett.* **2003**, *63* (2), 247−253.
(61) Putnam, S. A.; Cahill, D. G.; Wong, G. C. L. Temperature Dependence of Thermodiffusion in Aqueous Suspensions of Charged Nanoparticles. *Langmuir* **2007**, *23* (18), 9221−9228.
(62) Iacopini, S.; Rusconi, R.; Piazza, R. The "Macromolecular Tourist": Universal Temperature Dependence of Thermal Diffusion in Aqueous Colloidal Suspensions. *Eur. Phys. J. E: Soft Matter Biol. Phys.* **2006**, *19* (1), 59−67.
(63) Duhr, S.; Braun, D. Why Molecules Move Along a Temperature Gradient. *Proc. Natl. Acad. Sci. U. S. A.* **2006**, *103* (52), 19678−19682.
(64) Ning, H.; Dhont, J. K.; Wiegand, S. Thermal-Diffusive Behavior of a Dilute Solution of Charged Colloids. *Langmuir* **2008**, *24* (6), 2426−2432.
(65) Guthrie, G., Jr.; Wilson, J. N.; Schomaker, V. Theory of the Thermal Diffusion of Electrolytes in a Clusius Column. *J. Chem. Phys.* **1949**, *17* (3), 310−313.
(66) Eastman, E. Theory of the Soret Effect. *J. Am. Chem. Soc.* **1928**, *50* (2), 283−291.
(67) Helfand, E.; Kirkwood, J. G. Theory of the Heat of Transport of Electrolytic Solutions. *J. Chem. Phys.* **1960**, *32* (3), 857−866.
(68) Bresme, F.; Lervik, A.; Bedeaux, D.; Kjelstrup, S. Water Polarization under Thermal Gradients. *Phys. Rev. Lett.* **2008**, *101* (2), 020602.
(69) Di Lecce, S.; Bresme, F. Thermal Polarization of Water Influences the Thermoelectric Response of Aqueous Solutions. *J. Phys. Chem. B* **2018**, *122* (5), 1662−1668.
(70) Majee, A.; Würger, A. Thermocharge of a Hot Spot in an Electrolyte Solution. *Soft Matter* **2013**, *9* (7), 2145−2153.
(71) Reichl, M.; Herzog, M.; Götz, A.; Braun, D. Why Charged Molecules Move across a Temperature Gradient: The Role of Electric Fields. *Phys. Rev. Lett.* **2014**, *112* (19), 198101.
(72) Vigolo, D.; Rusconi, R.; Stone, H. A.; Piazza, R. Thermophoresis: Microfluidics Characterization and Separation. *Soft Matter* **2010**, *6* (15), 3489−3493.
(73) Parola, A.; Piazza, R. Particle Thermophoresis in Liquids. *Eur. Phys. J. E: Soft Matter Biol. Phys.* **2004**, *15* (3), 255−263.
(74) Anderson, J. L. Colloid Transport by Interfacial Forces. *Annu. Rev. Fluid Mech.* **1989**, *21* (1), 61−99.
(75) Landau, L. D.; Bell, J.; Kearsley, M.; Pitaevskii, L.; Lifshitz, E.; Sykes, J. *Electrodynamics of Continuous Media*; Elsevier: 2013; Vol. *8*.
(76) Dukhin, S. S.; Derjaguin, B. *Surface and Colloid Science*; Wiley-Interscience: 1974.

(77) Ramos, A.; Morgan, H.; Green, N. G.; Castellanos, A. Ac Electrokinetics: A Review of Forces in Microelectrode Structures. *J. Phys. D: Appl. Phys.* **1998**, *31* (18), 2338.
(78) Fayolle, S.; Bickel, T.; Würger, A. Thermophoresis of Charged Colloidal Particles. *Phys. Rev. E* **2008**, *77* (4), 041404.
(79) Rasuli, S. N.; Golestanian, R. Soret Motion of a Charged Spherical Colloid. *Phys. Rev. Lett.* **2008**, *101* (10), 108301.
(80) Ruckenstein, E. Can Phoretic Motions Be Treated as Interfacial Tension Gradient Driven Phenomena? *J. Colloid Interface Sci.* **1981**, *83* (1), 77−81.
(81) Bregulla, A. P.; Würger, A.; Günther, K.; Mertig, M.; Cichos, F. Thermo-Osmotic Flow in Thin Films. *Phys. Rev. Lett.* **2016**, *116* (18), 188303.
(82) Das, P. K. Effect of Thermodiffusion on Ph-Regulated Surface Charge Properties of Nanoparticle. *Electrophoresis* **2016**, *37* (2), 347−355.
(83) Armstrong, J.; Lervik, A.; Bresme, F. Enhancement of the Thermal Polarization of Water Via Heat Flux and Dipole Moment Dynamic Correlations. *J. Phys. Chem. B* **2013**, *117* (47), 14817−14826.
(84) Agar, J.; Mou, C.; Lin, J. L. Single-Ion Heat of Transport in Electrolyte Solutions: A Hydrodynamic Theory. *J. Phys. Chem.* **1989**, *93* (5), 2079−2082.
(85) Morthomas, J.; Würger, A. Thermophoresis at a Charged Surface: The Role of Hydrodynamic Slip. *J. Phys.: Condens. Matter* **2009**, *21* (3), 035103.
(86) Fayolle, S.; Bickel, T.; Le Boiteux, S.; Würger, A. Thermodiffusion of Charged Micelles. *Phys. Rev. Lett.* **2005**, *95* (20), 208301.
(87) Ghofraniha, N.; Ruocco, G.; Conti, C. Collective Thermal Diffusion of Silica Colloids Studied by Nonlinear Optics. *Langmuir* **2009**, *25* (21), 12495−12500.
(88) Gomes, R. C.; da Silva, A. F.; Kouyaté, M.; Demouchy, G.; Mériguet, G.; Aquino, R.; Dubois, E.; Nakamae, S.; Roger, M.; Depeyrot, J. Thermodiffusion of Repulsive Charged Nanoparticles-the Interplay between Single-Particle and Thermoelectric Contributions. *Phys. Chem. Chem. Phys.* **2018**, *20* (24), 16402−16413.
(89) Ning, H.; Buitenhuis, J.; Dhont, J. K.; Wiegand, S. Thermal Diffusion Behavior of Hard-Sphere Suspensions. *J. Chem. Phys.* **2006**, *125* (20), 204911.
(90) Huang, B.; Roger, M.; Bonetti, M.; Salez, T.; Wiertel-Gasquet, C.; Dubois, E.; Cabreira Gomes, R.; Demouchy, G.; Mériguet, G.; Peyre, V. Thermoelectricity and Thermodiffusion in Charged Colloids. *J. Chem. Phys.* **2015**, *143* (5), 054902.
(91) Sugioka, H. Nonlinear Thermokinetic Phenomena Due to the Seebeck Effect. *Langmuir* **2014**, *30* (28), 8621−8630.
(92) De Graaf, J.; Samin, S. Self-Thermoelectrophoresis at Low Salinity. *Soft Matter* **2019**, *15* (36), 7219−7236.
(93) Simoncelli, S.; Summer, J.; Nedev, S.; Kühler, P.; Feldmann, J. Combined Optical and Chemical Control of a Microsized Photofueled Janus Particle. *Small* **2016**, *12* (21), 2854−2858.
(94) Caldwell, D. R. Measurement of Negative Thermal Diffusion Coefficients by Observing the Onset of Thermohaline Convection. *J. Phys. Chem.* **1973**, *77* (16), 2004−2008.
(95) Gaeta, F.; Perna, G.; Scala, G.; Bellucci, F. Nonisothermal Matter Transport in Sodium Chloride and Potassium Chloride Aqueous Solutions. 1. Homogeneous System (Thermal Diffusion). *J. Phys. Chem.* **1982**, *86* (15), 2967−2974.
(96) Dhont, J. K.; Wiegand, S.; Duhr, S.; Braun, D. Thermodiffusion of Charged Colloids: Single-Particle Diffusion. *Langmuir* **2007**, *23* (4), 1674−1683.
(97) Forsythe, E. L.; Judge, R. A.; Pusey, M. L. Tetragonal Chicken Egg White Lysozyme Solubility in Sodium Chloride Solutions. *J. Chem. Eng. Data* **1999**, *44* (3), 637−640.
(98) Dietzel, M.; Hardt, S. Thermoelectricity in Confined Liquid Electrolytes. *Phys. Rev. Lett.* **2016**, *116* (22), 225901.
(99) Kotnala, A.; Kollipara, P. S.; Zheng, Y. Opto-Thermoelectric Speckle Tweezers. *Nanophotonics* **2020**, *9*, 927.
(100) Grigorenko, A. N.; Roberts, N. W.; Dickinson, M. R.; Zhang, Y. Nanometric Optical Tweezers Based on Nanostructured Substrates. *Nat. Photonics* **2008**, *2* (6), 365−370.
(101) Lu, J.; Yang, H.; Zhou, L.; Yang, Y.; Luo, S.; Li, Q.; Qiu, M. Light-Induced Pulling and Pushing by the Synergic Effect of Optical Force and Photophoretic Force. *Phys. Rev. Lett.* **2017**, *118* (4), 043601.
(102) Smalley, D.; Nygaard, E.; Squire, K.; Van Wagoner, J.; Rasmussen, J.; Gneiting, S.; Qaderi, K.; Goodsell, J.; Rogers, W.; Lindsey, M. A Photophoretic-Trap Volumetric Display. *Nature* **2018**, *553* (7689), 486−490.
(103) Lee, E.; Huang, D.; Luo, T. Ballistic Supercavitating Nanoparticles Driven by Single Gaussian Beam Optical Pushing and Pulling Forces. *Nat. Commun.* **2020**, *11* (1), 2404.
(104) Lee, E.; Luo, T. Long-Distance Optical Pulling of Nanoparticle in a Low Index Cavity Using a Single Plane Wave. *Science Advances* **2020**, *6* (21), No. eaaz3646.
(105) Li, J.; Hill, E. H.; Lin, L.; Zheng, Y. Optical Nanoprinting of Colloidal Particles and Functional Structures. *ACS Nano* **2019**, *13* (4), 3783−3795.
(106) Peng, X.; Li, J.; Lin, L.; Liu, Y.; Zheng, Y. Opto-Thermophoretic Manipulation and Construction of Colloidal Superstructures in Photocurable Hydrogels. *ACS Applied Nano Materials* **2018**, *1* (8), 3998−4004.
(107) Duhr, S.; Braun, D. Thermophoretic Depletion Follows Boltzmann Distribution. *Phys. Rev. Lett.* **2006**, *96* (16), 168301.
(108) Edwards, T. D.; Bevan, M. A. Depletion-Mediated Potentials and Phase Behavior for Micelles, Macromolecules, Nanoparticles, and Hydrogel Particles. *Langmuir* **2012**, *28* (39), 13816−13823.
(109) Gargiulo, J.; Brick, T.; Violi, I. L.; Herrera, F. C.; Shibanuma, T.; Albella, P.; Requejo, F. G.; Cortes, E.; Maier, S. A.; Stefani, F. D. Understanding and Reducing Photothermal Forces for the Fabrication of Au Nanoparticle Dimers by Optical Printing. *Nano Lett.* **2017**, *17* (9), 5747−5755.
(110) Rodrigo, J. A. Fast Optoelectric Printing of Plasmonic Nanoparticles into Tailored Circuits. *Sci. Rep.* **2017**, *7*, 46506.
(111) Lin, L.; Peng, X.; Mao, Z.; Li, W.; Yogeesh, M. N.; Rajeeva, B. B.; Perillo, E. P.; Dunn, A. K.; Akinwande, D.; Zheng, Y. Bubble-Pen Lithography. *Nano Lett.* **2016**, *16* (1), 701−708.
(112) Alam, M. S.; Zhan, Q.; Zhao, C. Additive Opto-Thermomechanical Nanoprinting and Nanorepairing under Ambient Conditions. *Nano Lett.* **2020**, *20* (7), 5057−5064.
(113) Qian, B.; Montiel, D.; Bregulla, A.; Cichos, F.; Yang, H. Harnessing Thermal Fluctuations for Purposeful Activities: The Manipulation of Single Micro-Swimmers by Adaptive Photon Nudging. *Chemical Science* **2013**, *4* (4), 1420−1429.
(114) Dai, B.; Wang, J.; Xiong, Z.; Zhan, X.; Dai, W.; Li, C.-C.; Feng, S.-P.; Tang, J. Programmable Artificial Phototactic Microswimmer. *Nat. Nanotechnol.* **2016**, *11* (12), 1087.
(115) Xuan, M.; Wu, Z.; Shao, J.; Dai, L.; Si, T.; He, Q. Near Infrared Light-Powered Janus Mesoporous Silica Nanoparticle Motors. *J. Am. Chem. Soc.* **2016**, *138* (20), 6492−6497.
(116) Xuan, M.; Shao, J.; Gao, C.; Wang, W.; Dai, L.; He, Q. Self-Propelled Nanomotors for Thermomechanically Percolating Cell Membranes. *Angew. Chem., Int. Ed.* **2018**, *57* (38), 12463−12467.
(117) Yang, P. P.; Zhai, Y. G.; Qi, G. B.; Lin, Y. X.; Luo, Q.; Yang, Y.; Xu, A. P.; Yang, C.; Li, Y. S.; Wang, L. Nir Light Propulsive Janus-Like Nanohybrids for Enhanced Photothermal Tumor Therapy. *Small* **2016**, *12* (39), 5423−5430.
(118) Soler, L.; Sánchez, S. Catalytic Nanomotors for Environmental Monitoring and Water Remediation. *Nanoscale* **2014**, *6* (13), 7175−7182.
(119) Šípová-Jungová, H.; Andrén, D.; Jones, S.; Käll, M. Nanoscale Inorganic Motors Driven by Light: Principles, Realizations, and Opportunities. *Chem. Rev.* **2020**, *120*, 269.
(120) Villa, K.; Pumera, M. Fuel-Free Light-Driven Micro/Nanomachines: Artificial Active Matter Mimicking Nature. *Chem. Soc. Rev.* **2019**, *48* (19), 4966−4978.

https://dx.doi.org/10.1021/acs.langmuir.0c03182
Langmuir 2021, 37, 1315−1336

(121) Wu, Z.; Chen, X.; Wang, M.; Dong, J.; Zheng, Y. High-Performance Ultrathin Active Chiral Metamaterials. *ACS Nano* **2018**, *12* (5), 5030−5041.
(122) Wu, Z.; Li, J.; Zhang, X.; Redwing, J. M.; Zheng, Y. Room-Temperature Active Modulation of Valley Dynamics in a Monolayer Semiconductor through Chiral Purcell Effects. *Adv. Mater.* **2019**, *31* (49), 1904132.
(123) Lin, L.; Lepeshov, S.; Krasnok, A.; Jiang, T.; Peng, X.; Korgel, B. A.; Alù, A.; Zheng, Y. All-Optical Reconfigurable Chiral Meta-Molecules. *Mater. Today* **2019**, *25*, 10−20.
(124) Haydon, D. The Surface Charge of Cells and Some Other Small Particles as Indicated by Electrophoresis: I. The Zeta Potential-Surface Charge Relationships. *Biochim. Biophys. Acta* **1961**, *50* (3), 450−457.
(125) Faraudo, J.; Bresme, F. Origin of the Short-Range, Strong Repulsive Force between Ionic Surfactant Layers. *Phys. Rev. Lett.* **2005**, *94* (7), 077802.
(126) Rica, R. A.; Bazant, M. Z. Electrodiffusiophoresis: Particle Motion in Electrolytes under Direct Current. *Phys. Fluids* **2010**, *22* (11), 112109.
(127) Cárdenas, M.; Schillén, K.; Nylander, T.; Jansson, J.; Lindman, B. DNA Compaction by Cationic Surfactant in Solution and at Polystyrene Particle Solution Interfaces: A Dynamic Light Scattering Study. *Phys. Chem. Chem. Phys.* **2004**, *6* (7), 1603−1607.
(128) Lu, F.; Kuai, Y.; Chen, J.; Tang, X.; Xiang, Y.; Liu, Y.; Wang, P.; Lakowicz, J. R.; Zhang, D. Switchable Assembly and Guidance of Colloidal Particles on an All-Dielectric One-Dimensional Photonic Crystal. *Phys. Rev. Appl.* **2020**, *13* (1), 014020.
(129) Wu, Z.; Kelp, G.; Yogeesh, M. N.; Li, W.; McNicholas, K. M.; Briggs, A.; Rajeeva, B. B.; Akinwande, D.; Bank, S. R.; Shvets, G.; Zheng, Y. Dual-Band Moiré Metasurface Patches for Multifunctional Biomedical Applications. *Nanoscale* **2016**, *8* (43), 18461−18468.
(130) Xiao, S.; Wang, T.; Liu, T.; Zhou, C.; Jiang, X.; Zhang, J. Active Metamaterials and Metadevices: A Review. *J. Phys. D: Appl. Phys.* **2020**, *53* (50), 503002.
(131) Maier, C. M.; Huergo, M. A.; Milosevic, S.; Pernpeintner, C.; Li, M.; Singh, D. P.; Walker, D.; Fischer, P.; Feldmann, J.; Lohmüller, T. Optical and Thermophoretic Control of Janus Nanopen Injection into Living Cells. *Nano Lett.* **2018**, *18* (12), 7935−7941.
(132) Kim, Y.; Ding, H.; Zheng, Y. Enhancing Surface Capture and Sensing of Proteins with Low-Power Optothermal Bubbles in a Biphasic Liquid. *Nano Lett.* **2020**, *20* (10), 7020−7027.
(133) Herms, A.; Günther, K.; Sperling, E.; Heerwig, A.; Kick, A.; Cichos, F.; Mertig, M. Concept, Synthesis, and Structural Characterization of DNA Origami Based Self-Thermophoretic Nanoswimmers. *Phys. Status Solidi A* **2017**, *214* (9), 1600957.
(134) Simoncelli, S.; Johnson, S.; Kriegel, F.; Lipfert, J.; Feldmann, J. Stretching and Heating Single Dna Molecules with Optically Trapped Gold-Silica Janus Particles. *ACS Photonics* **2017**, *4* (11), 2843−2851.

https://dx.doi.org/10.1021/acs.langmuir.0c03182
Langmuir 2021, 37, 1315−1336